

Light-induced breaking of symmetry in photonic crystal waveguides with nonlinear defects as a key for all-optical switching circuits

Evgeny Bulgakov, Almas Sadreev, and Konstantin N. Pichugin
Kirensky Institute of Physics, 660036, Krasnoyarsk, Russia
 (Dated: October 27, 2011)

We consider light transmission in 2D photonic crystal waveguide coupled with two identical nonlinear defects positioned symmetrically aside the waveguide. We show that with growth of injected light power there is a breaking of symmetry by two ways. In the first way the symmetry is broken because of different light intensities at the defects. In the second way the intensities at the defects are equal but phases of complex amplitudes are different. That results in a vortical power flow between the defects similar to the DC Josephson effect if the input power over the waveguide is applied and the defects are coupled. As application of these phenomena we consider the symmetry breaking for the light transmission in a T-shaped photonic waveguide with two nonlinear defects. We demonstrate as this phenomenon can be explored for all-optical switching of light transmission from the left output waveguide to the right one by application of input pulses. Finally we consider the symmetry breaking in the waveguide coupled with single defect presented however by two dipole modes.

PACS numbers:

I. INTRODUCTION

Symmetry breaking in a nonlinear quantum system is a fundamental effect caused by the interplay of nonlinearity with linear potential which defines the symmetry. It is commonly known that the ground state in one-dimensional linear quantum mechanics is nodeless and follows the symmetry of the potential. However the self-attractive nonlinearity in the nonlinear Schrödinger equation breaks the symmetry of the ground state, replacing it by a new asymmetric state minimizing the systems energy. For example, the nonlinear Schrödinger equation in double-well potential reveals anti-symmetric ground state with variation of normalization of the state [1]. The phenomenon of the spontaneous symmetry breaking in analog with the double-well potential are realized in a nonlinear dual-core directional fiber [2–4]. Spontaneous symmetry breaking was demonstrated recently by Brazhnyi and Malomed in a linear discrete chain (Schrödinger lattice) with two nonlinear sites [5]. They have shown as analytically as well as numerically the existence of symmetric, anti-symmetric, and non-symmetric eigen-modes with eigen-frequencies below the propagation band of the chain, and that a variation of the population of modes can give rise to a bifurcation from one to another mode. The system has direct relation to photonic crystal (PhC) waveguides with two in-channel nonlinear cavities where the population of the cavities might be governed by external source of the light.

Indeed, the phenomenon of symmetry breaking is studied in the nonlinear optics with injection of input power with the establishment of one or more asymmetric states which no longer preserve the symmetry properties of the original state [6–10]. In particular Maes *et al.* [11, 12] considered the symmetry breaking for the nonlinear cavities aligned along the waveguide, that is a Fabry-Pérot architecture close to the system considered in Ref. [8]. That system is symmetric relative to the inversion of the transport axis if equal power is injected on both sides of the coupled cavities. The symmetry breaking was found also for the case of many coupled nonlinear optical cavities in ring-like architecture [13, 14]. In the section II we write the equations of motion for the nonlinear optical cavities coupled with PhC waveguides by using an analogy of the two-dimensional PhC with quantum mechanics [15]. As for an application we consider three simple PhC systems which undergo the symmetry breaking phenomena for variation of the light frequency or the input power. The first simplest system is two identical nonlinear defects positioned symmetrically aside the straight forward linear waveguide (section III). Each defect is presented by single monopole mode. We show two types of the symmetry breaking [16, 17]. In the first type the symmetry is broken because of different light intensities at the defects. In the second type of the symmetry breaking the intensities at the cavities are equal but phases of complex amplitudes are different. That results in a vortical power flow between the defects similar to the DC Josephson effect if the input power over the waveguide is applied, and the defects are coupled.

In section IV we consider as the phenomenon of the symmetry breaking can be explored for so called all-optical switching [18–21] by use of the T-shaped photonic waveguide with two identical nonlinear cavities positioned symmetrically. That system combines two systems. The first one is the Fabry-Pérot interferometer (FPI) consisting of two nonlinear off-channel cavities aligned along the straightforward waveguide considered in Refs. [11, 12, 22]. As was shown in Ref. [22] there is a discrete set of the a self-induced bound (localized) states in continuum (BSC) which are the standing waves between off-channel cavities. In the second system two nonlinear cavities are aligned perpendicular to the input waveguide. As was said above there is the anti-bonding bound state in continuum (BSC). Here we show

that both types of the bound states might be important for the breaking of symmetry. All these phenomena agree well with computations based on an expansion of the electromagnetic field into optimally adapted photonic Wannier functions in two-dimensional PhC [23, 24].

Finally, in section V we consider the single nonlinear defect with two dipole eigen-modes which belong the propagation band of the PhC straightforward waveguide (section III). We demonstrate the symmetry breaking provided that the system is excited with equal powers from both sides similar to that Maes *et al.* has shown in the system of two coupled nonlinear cavities [11, 12].

II. BASIC EQUATIONS

The light propagation in linear PhC is described by the Maxwell equations

$$\begin{aligned}\nabla \times \vec{E} &= -\frac{\partial \vec{H}}{\partial t} \\ \nabla \times \vec{H} &= \frac{\partial \vec{D}}{\partial t}, \\ \vec{D}(\vec{r}, t) &= \epsilon_0(\vec{r})\vec{E}(\vec{r}, t).\end{aligned}\tag{1}$$

We take the light velocity to be equal to unit. However if there are defects with instantaneous Kerr nonlinearity, the displacement electric vector interior to the defects has a nonlinear contribution $\vec{D}(\vec{r}, t) = \epsilon_0(\vec{r})\vec{E}(\vec{r}, t) + \chi^{(3)}[\vec{E}(\vec{r}, t)]^2\vec{E}(\vec{r}, t)$ [25, 26]. A substitution of the electric field in the form $[\vec{E}(\vec{r}, t) = \frac{1}{2}[\vec{E}(\vec{r})e^{i\omega t} + \vec{E}^*(\vec{r})e^{-i\omega t}]]$ into Eq. (1) and neglect by highly oscillating terms such as $e^{2i\omega}$ allows us to write the Maxwell equations in the same form as Eq. (1) with

$$\epsilon(\vec{r}) = \epsilon_0(\vec{r}) + \frac{1}{4}\chi^{(3)}(\omega)|\vec{E}(\vec{r})|^2\vec{E}(\vec{r}) + \frac{1}{2}\chi^{(3)}(\omega)\vec{E}^2(\vec{r})\vec{E}^*(\vec{r}).\tag{2}$$

In what follows we consider the 2D PhC with arrays of infinitely long dielectric rods as shown in Fig. 1(a) in which the electric field is directed along the rods while the magnetic field is directed perpendicular to the rods [in the plane of Fig. 1(a)]. Then Eq. (2) simplifies as follows [25]

$$\epsilon(\vec{r}) = \epsilon_0(\vec{r}) + \frac{3}{4}\chi^{(3)}(\omega)|\vec{E}(\vec{r})|^2\vec{E}(\vec{r}).\tag{3}$$

There is a remarkable analogy of electrodynamics in dielectric media with quantum mechanics [15, 27]. In particular, if the nonlinear contribution to the dielectric constant is small we can use the well-known methods of quantum mechanical perturbation theory. Let $|\psi\rangle = \begin{pmatrix} \vec{E} \\ \vec{H} \end{pmatrix}$ be the electromagnetic state in the PhC. Then the Maxwell equations (1) can be written as the Schrödinger equation $i|\dot{\psi}\rangle = \hat{H}|\psi\rangle$ indeed with the Hamiltonian [15, 27, 28]

$$\hat{H} = \begin{pmatrix} 0 & \frac{i}{\epsilon(\vec{r})}\nabla \times \\ -i\nabla \times & 0 \end{pmatrix}.\tag{4}$$

Because of the perturbation of the dielectric constant (3) the Hamiltonian can be presented as $\hat{H} = \hat{H}_0 + \hat{V}$ where

$$\hat{H}_0 = \begin{pmatrix} 0 & \frac{i}{\epsilon_0(\vec{r})}\nabla \times \\ -i\nabla \times & 0 \end{pmatrix}, \quad \hat{V} = \begin{pmatrix} 0 & i\delta\left(\frac{1}{\epsilon(\vec{r})}\right)\nabla \times \\ 0 & 0 \end{pmatrix},\tag{5}$$

and

$$\delta\left(\frac{1}{\epsilon(\vec{r})}\right) = \frac{1}{\epsilon(\vec{r})} - \frac{1}{\epsilon_0(\vec{r})}.\tag{6}$$

Let us introduce (following, for example, Refs. [28, 29]) the following inner product for the unperturbed system:

$$\langle\psi|\psi'\rangle = \frac{1}{2}\int[\epsilon_0(\vec{r})\vec{E}^*\vec{E}' + \vec{H}^*\vec{H}']d^3\vec{r}.\tag{7}$$

which obeys the following normalization and orthogonality conditions for the bound eigen-states of the unperturbed Hamiltonian $\hat{H}_0|\psi_m\rangle = \omega_m|\psi_m\rangle$

$$\langle\psi_n|\psi_{n'}\rangle = \frac{1}{2} \int [\epsilon_0(\vec{r})\vec{E}_n^*\vec{E}_{n'} + \vec{H}_n^*\vec{H}_{n'}]d^3\vec{r} = \int \epsilon_0(\vec{r})\vec{E}_n^*\vec{E}_{n'}d^3\vec{r} = \delta_{nn'}. \quad (8)$$

Then the matrix elements for the perturbation calculated by use of these eigen-states are

$$\langle m|V|n\rangle = \frac{\omega_n}{2} \int d^3\vec{r}\epsilon_0^2(\vec{r})\delta\left(\frac{1}{\epsilon(\vec{r})}\right)\vec{E}_m^*(\vec{r})\vec{E}_n(\vec{r}). \quad (9)$$

One can see that the matrix (9) is not Hermitian as was noted in Ref. [28]. The origin is that the unperturbed states obey the inner product (7) with the dielectric constant $\epsilon_0(\vec{r})$ while the eigen-states of the full Hamiltonian $\hat{H}_0 + \hat{V}$ obey the inner product with a different dielectric constant $\epsilon(\vec{r})$. Respectively, the Hamiltonian \hat{H} is non-Hermitian with the inner product (8).

In order to avoid this problem we must use the inner product which is not tied to a specific choice of the dielectric constant. One way, given in Ref. [15], is by using only the magnetic field for the state. Another way is to absorb the dielectric constant in the scalar product by a new function as $\vec{F} = \sqrt{\epsilon(\vec{r})}\vec{E}$. Then the inner product becomes

$$\langle\psi|\psi'\rangle = \frac{1}{2} \int [\vec{F}^*\vec{F}' + \vec{H}^*\vec{H}']d^3\vec{r}. \quad (10)$$

The value $\langle\psi|\psi\rangle = \frac{1}{2} \int [\epsilon(\vec{r})|\vec{E}|^2 + |\vec{H}|^2]d^3\vec{r}$ is proportional to the energy of EM field which is important for the derivation of the forthcoming coupled mode theory (CMT) equations. That technique changes the Maxwell equations as follows:

$$\begin{aligned} \nabla \times \frac{\vec{F}}{\sqrt{\epsilon(\vec{r})}} &= -\dot{\vec{H}} \\ \frac{1}{\sqrt{\epsilon(\vec{r})}}\nabla \times \vec{H} &= \dot{\vec{F}}. \end{aligned} \quad (11)$$

The Hamiltonian takes the following form

$$\hat{H}_0 = \begin{pmatrix} 0 & \frac{i}{\sqrt{\epsilon_0(\vec{r})}}\nabla \times \\ -i\nabla \times \frac{1}{\sqrt{\epsilon_0(\vec{r})}} & 0 \end{pmatrix}, \quad \hat{V} = \begin{pmatrix} 0 & i\delta\left(\frac{1}{\sqrt{\epsilon(\vec{r})}}\right)\nabla \times \\ -i\nabla \times \delta\left(\frac{1}{\sqrt{\epsilon(\vec{r})}}\right) & 0 \end{pmatrix}. \quad (12)$$

Now the eigen-states of the full Hamiltonian can be expanded over the eigen-states $|m\rangle = \begin{pmatrix} \vec{F}_m \\ \vec{H}_m \end{pmatrix}$ of the unperturbed Hamiltonian \hat{H}_0 where

$$\begin{aligned} \nabla \times \frac{\vec{F}_m}{\sqrt{\epsilon_0(\vec{r})}} &= i\omega_m\vec{H}_m \\ \nabla \times \vec{H}_m &= -i\omega_m\sqrt{\epsilon_0(\vec{r})}\vec{F}_m. \end{aligned} \quad (13)$$

Then we obtain from (9)

$$\langle m|V|n\rangle = \frac{(\omega_m + \omega_n)}{2} \int d^3\vec{r}\epsilon_0^{3/2}(\vec{r})\delta\left(\frac{1}{\sqrt{\epsilon(\vec{r})}}\right)E_m^*(\vec{r})E_n(\vec{r}). \quad (14)$$

One can see that the full Hamiltonian is Hermitian now.

If the nonlinear defect rods are thin enough, the dielectric constant (3) can be rewritten as follows

$$\epsilon_j(\mathbf{x}) = (\epsilon_0 + \frac{3}{4}\chi^{(3)}(\omega)|E(\mathbf{x})|^2)\sum_j\theta(\mathbf{x}-\mathbf{x}_j). \quad (15)$$

Here j enumerates the defects, $\theta = 1$ inside the defect rod and $\theta = 0$ outside. As was shown for the simple square lattice 2D PhC from thin GaAs dielectric rods [24] the resonance spectra in the PhC waveguide are located in a rather narrow frequency domain. Therefore, we neglect the frequency dependence in the nonlinear susceptibility $\chi^{(3)}(\omega)$ in the following. Assuming that the nonlinear contribution in Eq. (15) is small compared to ϵ_0 we obtain for the matrix elements (14) per unit length of the defect rods

$$\langle m|V|n\rangle \approx -\frac{3}{16\epsilon_0^{3/2}}\chi^{(3)}(\omega_m + \omega_n) \sum_j \int_{\sigma_j} d^2\mathbf{x} |E(\mathbf{x})|^2 E_m(\mathbf{x})^* E_n(\mathbf{x}). \quad (16)$$

In order to find electric fields at the defects we must constitute a way to excite the defect modes. Here we consider that the EM field propagates from the left along the straight forward waveguide, interacts with the nonlinear defects, reflects back and transmits to the right. Then the transmission process can be described by the CMT stationary equations [30–33]

$$[\omega - \sum_n (\omega_m \delta_{mn} + V_{mn} + i\Gamma_n)] A_m = i\sqrt{\Gamma_m} E_{in}. \quad (17)$$

These CMT equations, in fact, are the Lippmann-Schwinger equation [34, 35]

$$(\omega - \hat{H}_{eff})\Psi = i\hat{W}E_{in}. \quad (18)$$

where the complex matrix \hat{H}_{eff} equals

$$\hat{H}_{eff} = \hat{H}_0 + \hat{V} - i\hat{W}\hat{W}^+, \quad (19)$$

the columns of the matrix \hat{W} consists of coupling constants of the m -th eigen-mode with the p -th injecting wave $\sqrt{\Gamma_{mp}}$, and the column Ψ consists of the mode amplitudes A_m . The solution Ψ is given by inverse of the matrix $\omega - \hat{H}_{eff}$ where the matrix elements of the effective Hamiltonian \hat{H}_{eff} in turn depend on the mode amplitudes A_m . In order to write the equations of self-consistency for the amplitudes at the defects we expand the electric field at the j -th defect over eigen-modes $E(\mathbf{x}_j) = \sum_m A_m \psi_m(\mathbf{x}_j)$. That defines the equations of self-consistency after substitution into Eq. (17).

Finally, we present the transmission amplitude in the framework of the CMT [31, 32]

$$t = E_{in} - \hat{W}^+ \Psi. \quad (20)$$

III. LINEAR OPTICAL WAVEGUIDE COUPLED WITH TWO NONLINEAR OFF-CHANNEL CAVITIES ALIGNED SYMMETRICALLY

Two identical nonlinear defects positioned symmetrically relative to the single straight forward waveguide is one of the simplest systems in which the breaking of symmetry occurs [16, 17]. The system can easily be realized in 2D PhC as shown in Fig. 1 (a). The system is symmetric relative to the inversion of the y axis, as shown in Fig. 1(b), and thereby supplements the system in which two nonlinear cavities are aligned along the waveguide considered by Maes *et al* [11, 12]. That system is symmetric relative to the inversion of the x axis if equal power is injected on both sides of the waveguide.

Let each defect supports a localized non degenerate monopole solution for the TM mode only, which has the electric field component parallel to the infinitely long rods [15, 24]. Other solutions, (dipole, quadrupole, etc.) are assumed to be extended in the photonic crystal for the appropriate cavity radius and the dielectric constant [24, 36] and are thereby excluded from the consideration. Therefore, we have a two-level description for \hat{H}_0 with the eigen-frequencies

$$\omega_{s,a} = \omega_0 \pm u \quad (21)$$

where u is the coupling constant u . We denote the corresponding even (bonding) and odd (anti-bonding) eigen-modes as $\psi_{s,a}(\mathbf{x})$. Both modes for specific PhC are shown in Fig. 2. We pay attention that the frequency of the bonding (nodeless) mode is higher than the frequency of the anti-bonding mode with one nodal line.

Next, we assume that the EM wave which propagates along the waveguide obeys the symmetry of the total system. Therefore the wave might be only symmetrical relative to $y \rightarrow -y$ or anti-symmetrical. Respectively, the symmetric wave could excite only the bonding mode while the anti-bonding mode would remain as a hidden mode. Other words, the anti-bonding mode is the bound state in symmetrical continuum [34]. The same refers to the case of the

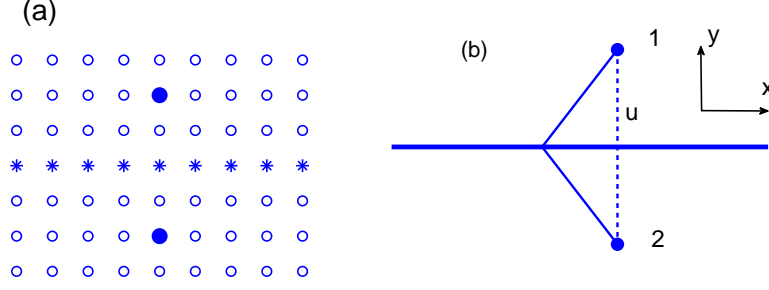


FIG. 1: (a) Two defect rods made from a Kerr media marked by filled circles are inserted into the square lattice PhC of dielectric rods with the lattice constant $a = 0.5\mu m$, the cylindrical dielectric rods have radius $0.18a$ and dielectric constant $\epsilon_0 = 11.56$. The 1D waveguide is formed by substitution of linear chain of rods by the rods with dielectric constant $\epsilon_W + \epsilon_0$ marked by stars. (b) Schematic system consisting of a waveguide aside coupled to two single-mode cavities. The cavities are coupled each other via u .

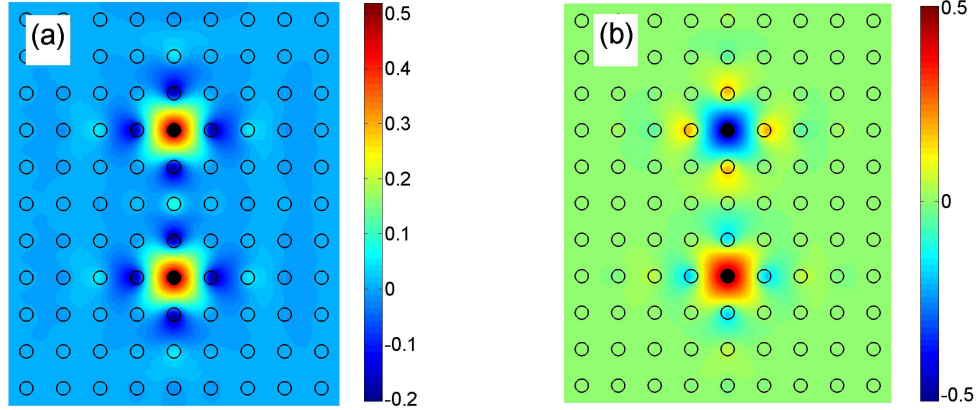


FIG. 2: (a) Bonding (even) mode and (b) anti-bonding (odd) mode of two overlapped linear defects in the 2D PhC. The defects have the same radius as the radius of rest rods but different dielectric constant $\epsilon_0 = 3$. The frequency of the isolated defect equals 0.3593 in terms of a value $2\pi c/a$. For the case of two overlapped defects shown here the frequency is split to be equal 0.3603 (bonding) and 0.3584 (anti-bonding).

anti-symmetric wave and the defect bonding mode. Therefore, for the linear case one can see the only resonance dip at ω_s , if the symmetric wave propagates along the waveguide. However due to the nonlinearity the light transmission acquires much more rich behavior because of spontaneous breaking of symmetry.

Substituting two eigen-functions $\psi_{s,a}(\mathbf{x})$ into Eq. (16) and considering a radius of the defect rods are very thin compared to the characteristic scale of wave function we obtain

$$\langle m|V|n \rangle \approx -\frac{3}{16}\sigma\chi^{(3)}(\omega_m + \omega_n) \sum_{j=1,2} |E(\mathbf{x}_j)|^2 \psi_m(\mathbf{x}_j)^* \psi_n(\mathbf{x}_j), \quad (22)$$

where σ is the cross-section of the defects. Finally, we obtain from Eq. (22)

$$\hat{V} = \lambda \begin{pmatrix} \omega_s \phi_s^2(I_1 + I_2) & \omega_0 \phi_s \phi_a(I_1 - I_2) \\ \omega_0 \phi_s \phi_a(I_1 - I_2) & \omega_a \phi_a^2(I_1 + I_2) \end{pmatrix} \quad (23)$$

where $\phi_s = \psi_s(\mathbf{x}_1)\sqrt{\sigma} = \psi_s(\mathbf{x}_2)\sqrt{\sigma}$, $\phi_a = \psi_a(\mathbf{x}_1)\sqrt{\sigma} = -\psi_a(\mathbf{x}_2)\sqrt{\sigma}$, \mathbf{x}_1 and \mathbf{x}_2 are the positions of the defects in the two-dimensional PhC, and $I_j = |E(\mathbf{x}_j)|^2$, $j = 1, 2$ are the intensities of the electric field at the nonlinear defects, $\lambda = -\frac{3}{4}\chi^{(3)}$.

In order to find electric fields at the defects we must constitute a way to excite the defect modes. Here we consider that the EM field propagates from the left along the waveguide, interacts with the nonlinear defects, reflects back, and transmits to the right. Then the transmission process can be described by the CMT stationary equations [30–32] for the bonding mode amplitude A_s and the anti-bonding amplitude A_a

$$\begin{aligned} [\omega - \omega_s - \lambda\omega_s\phi_s^2(I_1 + I_2) + i\Gamma]A_s - \lambda\omega_0\phi_s\phi_a(I_1 - I_2)A_a &= i\sqrt{\Gamma}E_{in}, \\ -\lambda\omega_0\phi_s\phi_a(I_1 - I_2)A_s + [\omega - \omega_a - \lambda\omega_a\phi_a^2(I_1 + I_2)]A_a &= 0, \end{aligned} \quad (24)$$

where only the bonding mode is coupled with the waveguide because of the symmetry. The equivalent model is shown in Fig. 1 (b).

The amplitudes A_s and A_a are given by inverse of the matrix given in the right hand of Eq. (24) whose matrix elements in turn depend on the intensities I_1, I_2 . In order to write the equations of self-consistency for the intensities at the defects $I_j, j = 1, 2$ we expand the electric field $E(\mathbf{x})$ at the thin j -th defect over eigen-modes $\phi_s(\mathbf{x})$ as $E(\mathbf{x}_j) = \sum_{m=s,a} A_m\phi_m(\mathbf{x}_j)$. The expansion can be specified as follows

$$E_1 = E(\mathbf{x}_1) = \phi_s A_s + \phi_a A_a, \quad E_2 = E(\mathbf{x}_2) = \phi_s A_s - \phi_a A_a \quad (25)$$

where symmetry properties of the eigen modes $\phi_m(\mathbf{x})$ were taken into account. Respectively,

$$I_1 = |\phi_s A_s + \phi_a A_a|^2, \quad I_2 = |\phi_s A_s - \phi_a A_a|^2 \quad (26)$$

which defines the equations of self-consistency after substitution into Eq. (24). In general they are rather cumbersome. Let us, first, consider the more simple case of the isolated defects so that the overlapping u can be neglected. Then the values of the eigen-functions at the defects are equal $\phi_s = \phi_a$. Even in that simplified case the solution of Eqs. (24) has cardinal features different from the case of the single nonlinear defect considered in Refs. [37–43]. These features are the result of the mutual interference of wave flows reflected by the nonlinear defects. If $\det(\hat{H}_{eff} - \omega) \neq 0$ the amplitudes of the mode excitement for the transmission can be easily found from Eq. (24) as follows

$$\begin{aligned} A_s &= \frac{i\sqrt{\Gamma}E_{in}[\omega - \omega_0(1 + 2\lambda I)]}{(\omega - \omega_0(1 + 2\lambda I))^2 - \omega_0^2\Delta^2 + i\Gamma(\omega - \omega_0(1 + 2\lambda I))}, \\ A_a &= \frac{i\sqrt{\Gamma}E_{in}\omega_0\Delta}{(\omega - \omega_0(1 + 2\lambda I))^2 - \omega_0^2\Delta^2 + i\Gamma(\omega - \omega_0(1 + 2\lambda I))}, \end{aligned} \quad (27)$$

where the values $I = (I_1 + I_2)/2, \Delta = \lambda(I_1 - I_2)$ in turn depend on the mode amplitudes according to (26). Substituting these solutions into Eq. (26) we obtain the following nonlinear equations of self-consistency

$$\begin{aligned} I_1 &= \frac{\Gamma E_{in}^2 [\omega - \omega_0(1 + 2\lambda I_2)]^2}{[\omega - \omega_0(1 + 2\lambda I_1)]^2 [\omega - \omega_0(1 + 2\lambda I_2)]^2 + \Gamma^2 [\omega - \omega_0(1 + 2\lambda I)]^2}, \\ I_2 &= \frac{\Gamma E_{in}^2 [\omega - \omega_0(1 + 2\lambda I_1)]^2}{[\omega - \omega_0(1 + 2\lambda I_1)]^2 [\omega - \omega_0(1 + 2\lambda I_2)]^2 + \Gamma^2 [\omega - \omega_0(1 + 2\lambda I)]^2}. \end{aligned} \quad (28)$$

The solution of these equations gives the steady state for the transmission in the waveguide coupled with two nonlinear defects. Finally, we write from Eq. (20) equation for the transmission amplitude:

$$t = E_{in} - \sqrt{\Gamma}A_s. \quad (29)$$

The odd amplitude A_a does not contribute into the transmission amplitude because of the symmetry.

In the forthcoming CMT calculations we fix the parameters of the CMT model as follows: $\omega_0 = 1, \Gamma = 0.01, \lambda = -0.01$. We consider the case of isolated defects $u = 0, \phi_s = \phi_a = 1$ and the case of coupled defects with $u = 0.01, \phi_s = 1, \phi_a = 1.1$. Rigorously speaking these values u and ϕ_s, ϕ_a correlate with each other. However, in our model case, we disregard this correlation.

A. Symmetry preserving solution

We start with the solution $E_1 = E_2$ that preserves the symmetry. In this case the incident wave excites only the symmetric even mode A_s

$$A_s = \frac{i\sqrt{\Gamma}E_{in}}{\omega - \omega_0(1 + 2\lambda I) + i\Gamma} \quad (30)$$

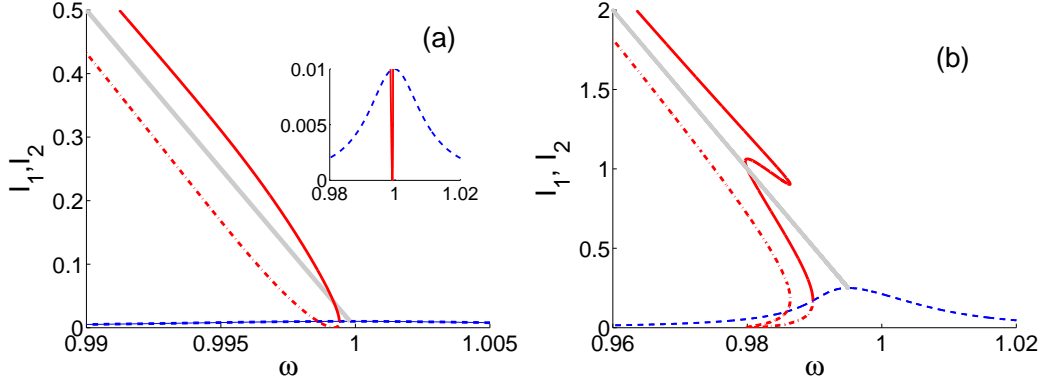


FIG. 3: Frequency behavior of the intensities at the isolated defects $u = 0$. (a) $E_{in} = 0.01$, (b) $E_{in} = 0.05$. Here and in the forthcoming figures dashed blue line shows the symmetry preserving solution. Solid and dash-dotted red lines show the symmetry breaking solutions which has different intensities at the defects I_1 and I_2 . Gray thick solid line shows a new phase parity breaking solution at which $\det(\omega - \hat{H}_{eff}) = 0$.

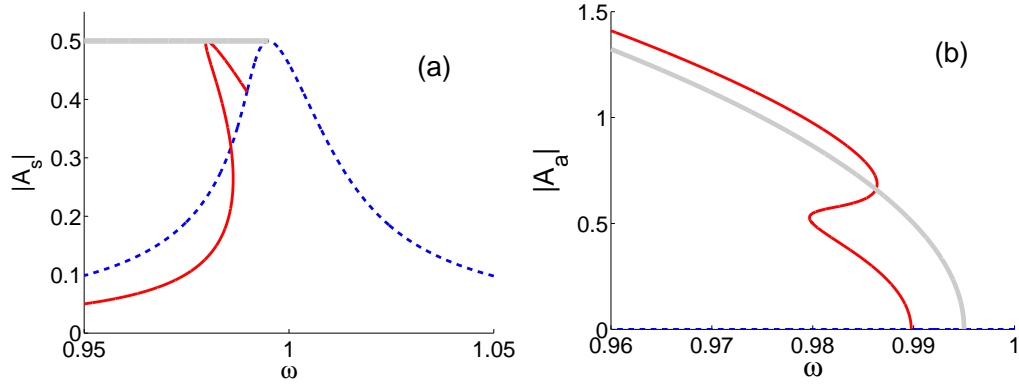


FIG. 4: Frequency behavior of (a) the bonding amplitude $|A_s|$ and (b) the anti-bonding amplitude $|A_a|$ of the model shown in Fig. 1 (b) for $u = 0$, $E_{in} = 0.05$.

as follows from Eq. (27) with the only resonance frequency $\omega_0(1 + 2\lambda I)$ and the width 2Γ . The self-consistency equation for the symmetry preserving solution $I = I_1 = I_2$ simplifies

$$I[(\omega - \omega_0(1 + 2\lambda I))^2 + \Gamma^2] = \Gamma E_{in}^2. \quad (31)$$

That coincides with the equation of self-consistency for the single off-channel nonlinear defect obtained in Ref. [38]. The solution of this cubic nonlinear equation is shown in Fig. 3 by dashed blue lines. The frequency behavior of the intensities inherits the linear case, as shown in the inset. With growth of the input power the resonance frequency shifts to the left because of the nonlinear contribution $2\lambda I$ as seen from Eq. (30).

The frequency behavior of mode excitations $|A_s|$, $|A_a|$ is shown in Fig. 4 by blue dashed lines. As seen from Fig. 4 (a) A_s has a resonance peak. Respectively, the transmission $T = |t|^2/E_{in}^2$ has a resonance dip at the frequency $\omega_0(1 + 2\lambda I) = \omega_0(1 + 2\lambda E_{in}^2/\Gamma)$ as shown in Fig. 5(a) by the dashed line. The last equality follows from Eq. (31).

B. Symmetry breaking solution

For the transmission through the nonlinear symmetric media the symmetry might be broken [6–14]. Numerical solution of Eq. (24), indeed, reveals the solution with $I_1 > I_2$, i.e., the nonlinearity gives rise to a breaking of the symmetry below (above) the critical frequency ω_c for $\lambda < 0$ ($\lambda > 0$). The symmetry breaking solution is shown in Fig. 3 by solid lines for I_1 and dash-dotted lines for I_2 . There is also the solution that differs from the former in that $E_1 \leftrightarrow E_2$. If the solutions are stable, a choice of the solution happens incidentally, as it does for a phase transition of

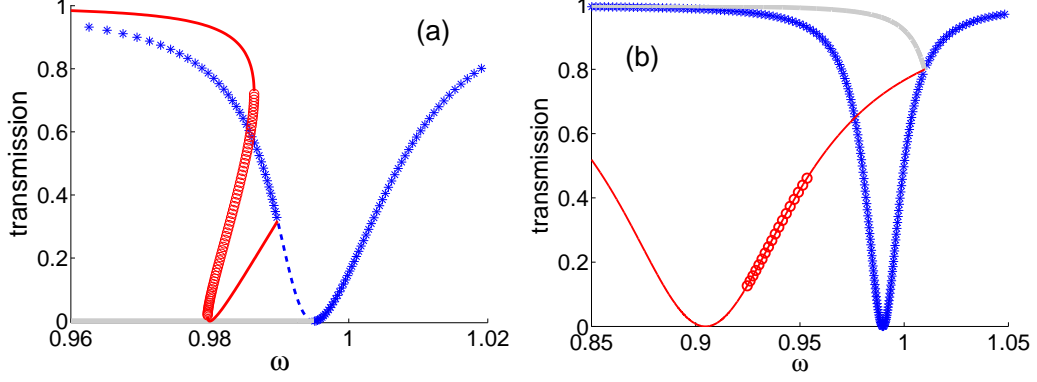


FIG. 5: Frequency behavior of the transmission for the isolated defects for (a) $E_{in} = 0.05$ and (b) for the coupled defects for $E_{in} = 0.01$. Stars and open circles show stable domains of the solutions.

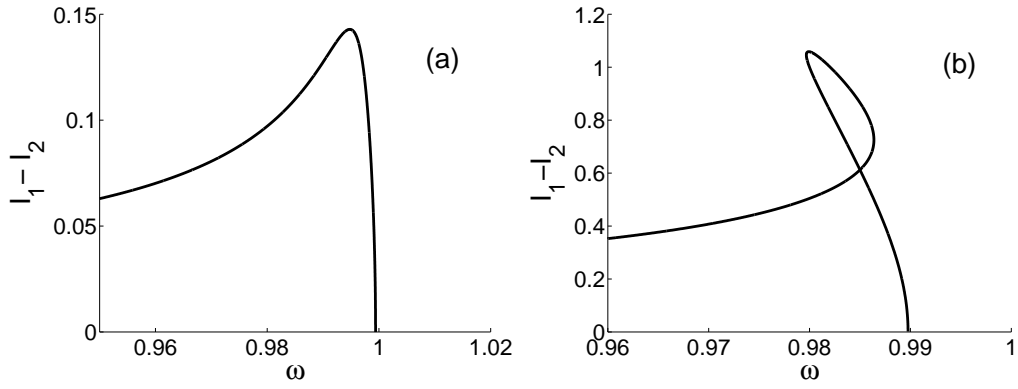


FIG. 6: The difference between the intensities at the defects for $u = 0$: (a) $E_{in} = 0.01$ and (b) $E_{in} = 0.05$. Only the symmetry breaking solution is shown.

the second order in cooperative systems. As shown in Fig. 6, a value $I_1 - I_2$ or the odd mode amplitude A_a , indeed, might serve as the order parameter that characterizes the symmetry breaking.

It is surprising that there is the frequency at which the intensity at one of the nonlinear defects turns to zero as shown in Fig. 3. According to Eqs. (28) that occurs at the frequency

$$\omega_{dip} = \omega_0(1 + 8\lambda E_{in}^2/\Gamma). \quad (32)$$

At this frequency we have $A_s = A_a = E_1/2 = E_{in}/\sqrt{\Gamma}$ in accordance with Eqs. (27) and (25). By substituting this equality into Eq. (20) we immediately obtain that the frequency (32) defines the position of resonance dip for the symmetry breaking solution. As will be shown, that result of full extinction of one of the nonlinear defects is observed in the PhC system as well [Fig. 13(b)].

In Figs. 4(a) and 4(b) we show the frequency dependence of the even and odd mode amplitudes $|A_s|$ and $|A_a|$ respectively for $E_{in} = 0.05$. One can see that, first, the incident wave begins to excite the odd mode below ω_c for $\lambda < 0$, and, second, $|A_s|$ and $|A_a|$ show the bistability. The even mode A_s displays a resonance peak (solid line) with the resonance width twice less than the resonance width of the peak for the symmetry preserving solution (dashed line). Correspondingly, the transmission in Fig. 5 demonstrates a narrow dip for the symmetry breaking solution. In order to understand that phenomenon let us consider the resonance poles of the even and odd amplitudes given by zeros of the denominators in Eq. (27)

$$z_{1,2} = \omega_0(1 + 2\lambda I) - \frac{i\Gamma}{2} \pm \sqrt{\omega_0^2 \Delta^2 - \frac{\Gamma^2}{4}}. \quad (33)$$

For the solution with $\Delta = 0$ we had the only resonance pole with the resonance half width Γ . As Fig. 6 shows there is the frequency domain roughly between 0.98 and 0.99 where $\omega_0 \Delta > \Gamma/2$ and where the resonance half-width is twice

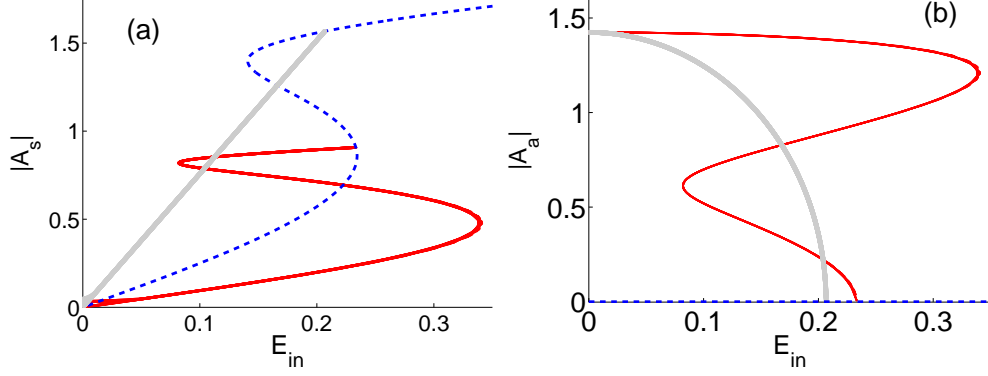


FIG. 7: Amplitudes (a) $|A_s|$ and (b) $|A_a|$ as a function of the incident wave amplitude E_{in} for the coupled defects with the parameters $\omega = 0.95$, $u = 0.01$, $\phi_s = 1$, $\phi_a = 1.1$.

less than Γ according to formula (33). Therefore, in this frequency domain we can expect the resonance dip to be twice narrower compared to the symmetry preserving solution with $\Delta = 0$.

The lesser the width of resonance, the more unstable the resonance [15]. One can thereby see that the bistability of the symmetry breaking solution is more profound in comparison to the symmetry preserving solution. The resonance peak in $|A_s|$ for the symmetry breaking solution terminates at that frequency where the odd mode amplitude $|A_a|$ arises as seen from Fig. 4(b). Close to this frequency the amplitude A_a has a square root behavior typical for the order parameter in phase transition of the second order. The dependence of A_a on the amplitude of the incident wave demonstrates the same behavior [see below Fig. 7 (b)].

C. Phase parity breaking solution

At last, there is the solution that has equal intensities at the defects but nevertheless a symmetry is broken because of phases of the complex amplitudes E_1 and E_2 . This solution refers to the special case of Eq. (24) when the determinant of the matrix $\omega - \hat{H}_{eff}$ equals zero, (i.e., the inverse of matrix does not exist). It occurs at

$$I_1 = I_2 = I, \quad \omega = \omega_a(1 + 2\lambda\phi_a^2 I). \quad (34)$$

Then the solution of Eq. (24) for the even mode amplitude A_s is

$$A_s = \frac{E_{in}}{\sqrt{\Gamma}}, \quad (35)$$

while A_a is undetermined yet.

Let us take for a while, the defects to be linear. Then the second equation in (34) shrinks to the isolated point $\omega = \omega_a$. As given by the CMT equations (24) and as seen from Fig. 1 this odd mode has zero overlapping with the waveguide and Eq. (34) thereby defines the bound state in continuum (BSC) [34, 44–48]. The solution of the Eq. (24) $\begin{pmatrix} A_s \\ A_a \end{pmatrix}$ with A_s given by Eq. (35) and arbitrary A_a is therefore a superposition of the transport solution and the BSC.

For the nonlinear defects the situation changes dramatically. First, there is the whole frequency region $\omega \geq \omega_a$ for $\lambda > 0$ or $\omega \leq \omega_a$ for $\lambda < 0$ where $\det(\omega - \hat{H}_{eff}) = 0$ as seen from Eq. (34). Equation (34) thereby defines the BSC with eigen frequency in whole region as dependent on the BSC intensity. Second, the BSC can not be independently superposed to the transport solution for the nonlinear case. The BSC begins to couple with the incident wave and can not be defined as the bound state if $E_{in} \neq 0$.

(i) Let the defects be isolated; (i.e. $u = 0$, $\phi_s = \phi_a = 1$). On the one hand, we obtain from Eq. (35)

$$A_s = \frac{E_1 + E_2}{2} = E_{in}/\sqrt{\Gamma}, \quad (36)$$

according to Eq. (25). That is the bonding mode amplitude is constant over the frequency as shown in Fig. 4 (a) by the gray thick solid line. On the other hand, Eq. (34) directly shows that the intensities at the defects do not depend

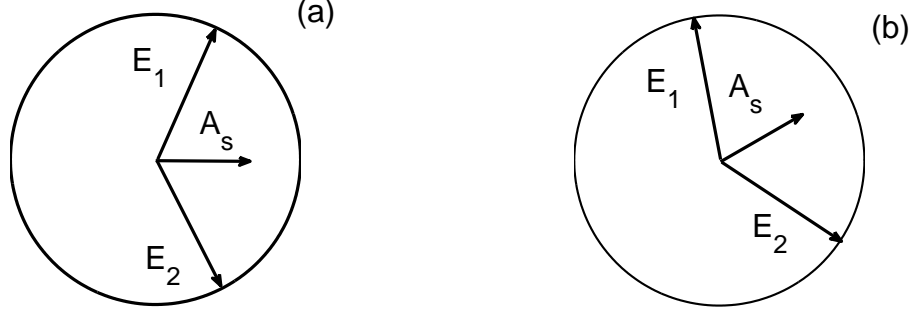


FIG. 8: Graphic solutions of (a) Eqs. (36) (a) and (40) (b), respectively. Radius of circle is \sqrt{I} .

on E_{in} ,

$$I = \frac{\omega - \omega_0}{2\lambda}. \quad (37)$$

Since $|E_1| = |E_2| = \sqrt{I}$ the only way to satisfy Eqs. (36) and (37) is to consider that the amplitudes at the defects are $E_1 = \sqrt{I} \exp(i\theta)$, $E_2 = \sqrt{I} \exp(-i\theta)$. That is illustrated in Fig. 8(a). With the use of Eqs. (36) and (37), we obtain

$$\cos^2 \theta = \frac{2\lambda E_{in}^2}{\Gamma(\omega - \omega_0)}. \quad (38)$$

For $E_{in} \rightarrow 0$ we have the following limits: $\theta \rightarrow \pi/2$, $E_1 \rightarrow i\sqrt{I}$, $E_2 \rightarrow -i\sqrt{I}$, $E_1 + E_2 \rightarrow 0$ as seen from Eq. (38). As soon as $E_{in} \neq 0$ the defects amplitudes are seized to oscillate in fully anti-symmetric way as shown in Fig. 8(a). We emphasize that phase difference 2θ has nontrivial behavior if the defects are nonlinear ($\lambda \neq 0$) and the incident wave is applied ($E_{in} \neq 0$) as follows from Eq. (38). For the symmetry preserving solution $\theta = 0$ (dashed line in Fig. 9), for the symmetry breaking solution $2\theta = 0$ or π (solid line in Fig. 9) while for the present solution the phase difference 2θ behaves as an order parameter (gray thick dashed line in Fig. 9) similar to A_a shown in Figs. 4(b) or 7(b).

We define the present solution of the CMT equations (24) with the zero determinant $\det(\omega - H_{eff}) = 0$ as the phase parity breaking solution. It exists for $\omega \leq \omega_0 + 2\lambda E_{in}^2/\Gamma$ for $\lambda < 0$. Knowledge of the phase θ allows us now to find the anti-bonding amplitude

$$A_a = (E_1 - E_2)/2 = i\sqrt{I} \sin \theta. \quad (39)$$

The frequency behavior of the even and odd amplitudes $|A_s|$, $|A_a|$ are shown in Figs. 4(b) and 7(b). Finally, by substituting Eq. (36) into Eq. (29) we obtain $t = 0$ for the phase parity breaking solution as shown in Fig. 5(a) by gray thick dashed line.

(ii) Coupled defects. For the PhC structure shown in Fig. 1(a) the coupling between the defects u is rather small compared to the coupling between the waveguide and defects \sqrt{I} . Nevertheless, an account of the coupling between the defects has a principal importance as will be seen below. As was given earlier, the parameters of the coupled defects are specified as follows $u = 0.01$, $\phi_s = 1$, $\phi_a = 1.1$.

A substitution of Eq. (34) into Eq. (35) gives

$$A_s = \frac{\omega_0 + u}{\omega_0(1 - \alpha) + u(1 + \alpha)} \cdot \frac{\sqrt{I} E_{in}}{\omega - \omega_r + i\Gamma_r} = \frac{A_{s0}}{\omega - \omega_r + i\Gamma_r} \quad (40)$$

where

$$\omega_r = \frac{(1 - \alpha)\omega_s\omega_a}{\omega_0(1 - \alpha) + u(1 + \alpha)}, \quad (41)$$

$$\Gamma_r = \Gamma \frac{\omega_a}{\omega_0(1 - \alpha) + u(1 + \alpha)}, \quad (42)$$

$$A_{s0} = \frac{\sqrt{I} E_{in} \omega_a}{\omega_0(1 - \alpha) + u(1 + \alpha)} \quad (43)$$

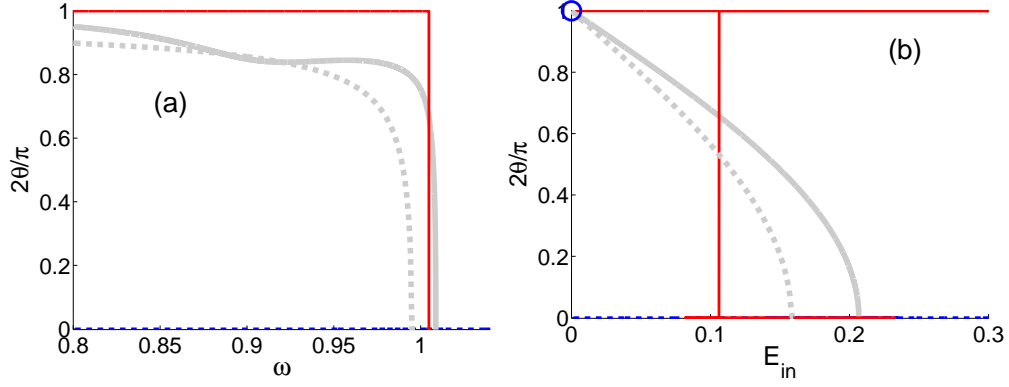


FIG. 9: Difference between phases of the amplitudes E_1 and E_2 for $u = 0.01$ as a function of (a) the frequency for $E_{in} = 0.05$ and (b) the amplitude of the incident wave for $\omega = 0.95$. Dashed blue line shows the symmetry preserving solution, solid red line shows the symmetry breaking solution, and gray lines show the phase parity breaking solution, $u = 0$ dashed and $u = 0.01$ solid. The BSC point is shown by open bold circle.

$\alpha = \phi_s^2/\phi_a^2$. Therefore for the coupled defects the amplitude A_s acquires typical Bright-Wigner resonance behavior in which the nonlinearity is excluded. Respectively, a substitution of the solution (40) into Eq. (29) immediately results in the transmission having the resonance dip at the frequency ω_r with the half width Γ_r which depends on ratio α and u . That result is shown in Fig. 5(b) by the gray thick line. If $u \rightarrow 0, \phi_a \rightarrow \phi_s, \alpha \rightarrow 1$ the frequency of the resonance dip goes away, and $\Gamma_r \rightarrow \infty$; that is, the resonance at the phase parity breaking solution disappears, and the corresponding transmission tends to zero as seen from Fig. 5(a).

Equation (34) fixes intensity at the defects

$$I = \frac{\omega - \omega_a}{2\lambda\phi_a^2\omega_a} \quad (44)$$

which is similar to the former case given by Eq. (37). On the other hand, we have according to Eq. (25) $E_1 + E_2 = A_s/2\phi_s$ where A_s is given by Eq. (40). A graphic illustration of the solution of this equation with modules of $E_j, j = 1, 2$ fixed by Eq. (44), is shown in Fig. 8(b). By presenting $E_1 = \sqrt{I} \exp(i(\beta + \theta))$ and $E_2 = \sqrt{I} \exp(i(\beta - \theta))$ we obtain from Eqs. (40)

$$\begin{aligned} \cos^2 \theta &= \frac{\lambda\Gamma_r\omega_a\omega_r E_{in}^2}{2\alpha(1-\alpha)\omega_s(\omega-\omega_a)[(\omega-\omega_r)^2 + \Gamma_r^2]}, \\ \tan \beta &= \frac{\omega - \omega_r}{\Gamma_r}. \end{aligned} \quad (45)$$

The behavior of the phase difference 2θ on the frequency or the incident wave amplitude E_{in} for $u = 0.01$ is shown in Fig. 9.

However, the most remarkable feature of the phase parity breaking solution for $u \neq 0$ is related in a current circulated between the defects. When the phase difference 2θ exists between two quantum dots (QD) or superconductors, connected by a weak link, a tunneling or Josephson current $J = J_0 \sin 2\theta$ will flow between them. The value of the current J_0 is proportional to the coupling constant between QDs or superconductors [49]. In order to explicitly write the expression for a current flowing between defects we use the Green function approach developed in Refs. [37, 39, 50] for the 2D PhC of dielectric rods with the dielectric constant ϵ_0 . The PhC holds the 1D cavity (waveguide) and two 0D defects (nonlinear cavity rods) as shown in Fig. 1 (a). Then the dielectric constant of full system $\epsilon(\mathbf{x})$ is a sum of periodic perfect PC and cavity-induced terms $\epsilon(\mathbf{x}) = \epsilon_{PC}(\mathbf{x}) + \delta\epsilon(\mathbf{x}|E)$, where $\delta\epsilon(\mathbf{x}|E) = \epsilon_W(\mathbf{x}) + \epsilon_d(\mathbf{x}|E)$ is contributed by the waveguide and the two nonlinear defects:

$$\epsilon_d(\mathbf{x}|E) = \epsilon_W \sum_{n=-\infty}^{\infty} \theta(\mathbf{x} - \mathbf{x}_n) + \sum_{j=1,2} \epsilon_j. \quad (46)$$

Here $\theta = 1$ inside the cavity rod and $\theta = 0$ outside, and the nonlinear contributions ϵ_j are given by Eq. (15). Then the TM electric field directed along the rods of the PhC $E(\mathbf{x}, t) = E(\mathbf{x})e^{i\omega t}$ is satisfied the integral equation

$$E(\mathbf{x}) = \frac{\omega^2}{c^2} \int d^2\mathbf{y} G(\mathbf{x}, \mathbf{y}|\omega) \delta\epsilon(\mathbf{y}|E) E(\mathbf{y}) \quad (47)$$

where $G(\mathbf{x}, \mathbf{y}|\omega)$ is the Green function of the ideal 2D PC of the rods which was calculated in Ref. [50] for the square lattice PhC. If the radius of the defects rods is sufficiently small in comparison to the wavelength of the EM wave, we can write Eq. (47) as the discrete nonlinear equation [39, 50]

$$E_{\mathbf{n}} = \sum_{\mathbf{m}} J_{\mathbf{n}-\mathbf{m}}(\omega) \delta\epsilon_{\mathbf{m}} E_{\mathbf{m}} \quad (48)$$

where $J_{\mathbf{n}-\mathbf{m}}(\omega) = \sigma \frac{\omega^2}{c^2} G(\mathbf{x}_{\mathbf{n}}, \mathbf{x}_{\mathbf{m}}|\omega)$, σ is the cross-section of the rods, and \mathbf{n}, \mathbf{m} runs over sites of the defects [marked by stars and filled circles in Fig. 1 (a)].

We use the nearest-neighbor approximation and write (48) as the tight-binding linear chain coupled with two nonlinear defects

$$\begin{aligned} [\frac{1}{\epsilon_W} - J_0(\omega)]E_n &= J_1(E_{n+1} + E_{n-1}) + \delta_{n,0} \frac{J_2}{\epsilon_W} (\delta\epsilon_1 E_1 + \delta\epsilon_2 E_2), \\ [1 - \delta\epsilon_1 J_0(\omega)]E_1 &= J_2 \epsilon_W E_0 + J_4 \delta\epsilon_2 E_2, \\ [1 - \delta\epsilon_2 J_0(\omega)]E_2 &= J_2 \epsilon_W E_0 + J_4 \delta\epsilon_1 E_1. \end{aligned} \quad (49)$$

The model is shown in Fig. 10 and consists of a linear infinitely long tight-binding chain presented by amplitudes E_n whose spectrum is given by dispersion equation $J_0(\omega) = \frac{1}{\epsilon_W} - 2J_1 \cos k$, and two nonlinear defects presented by amplitudes ϕ_1, ϕ_2 . The coupling J_2 connects the defects and the chain and the coupling J_4 connects the defects.

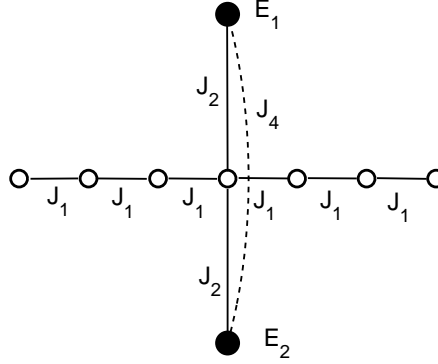


FIG. 10: Tight-binding version of the PhC system shown in Fig. 1 (a): J_2 couples the chain and the defects and J_4 connects the defects to each other.

By multiplying Eq. (49) by $E_0^* = t^*$ and subtracting the complex conjugated terms one can obtain the value of the power flow current flowing between the chain at the "0"-th site and the defects enumerated as $j = 1, 2$ as follows

$$j_{0 \rightarrow 1,2} = \epsilon_W J_2 \text{Im}(t E_{1,2}^*). \quad (50)$$

Similar manipulations with the cavity's amplitudes give the current between the defects

$$j_{1 \rightarrow 2} = J_4 \delta\epsilon \text{Im}(E_1 E_2^*) = J_4 \delta\epsilon I \sin(2\theta). \quad (51)$$

It follows also that the current from the "-1"-th site to the "0"-th site of the chain coincide with the current from the "0"-th site to the "1"-th one. Therefore the currents (50) and (51) coincide also in accordance to the Kirchhoff rule. Thus, the input power induces vortical current between the waveguide and defects via the couplings J_2 and J_4 . The current is excited by the incident wave provided the defects are nonlinear. Thus, our analysis shows that the symmetry can be broken not only because of different intensities at the defects but also by a circulating current between the defects although the intensities at the defects are equal. This model result of the Josephson like current between the defects with different phase is reflected in computations of the Poynting vector in the PhC structure as will be shown below.

D. Stability of solutions

Furthermore, we studied stability of different solutions by standard methods given for example in Ref. [29]. The stability of the solution can be found from the temporal CMT equations

$$i\dot{a}_s = [\omega_s + \lambda\omega_s\phi_s^2(I_1 + I_2) - i\Gamma]a_s + \lambda\omega_0\phi_s\phi_a(I_1 - I_2)a_a + \sqrt{\Gamma}E_{in}e^{-i\omega t},$$

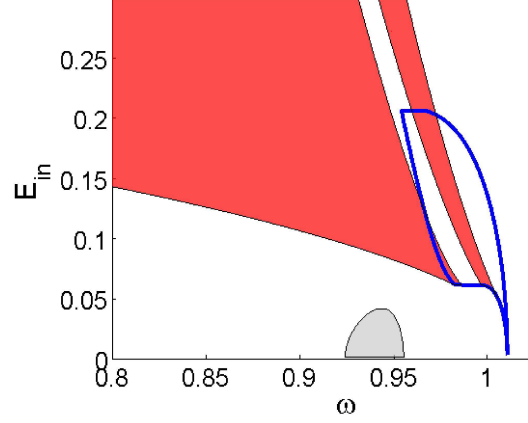


FIG. 11: Regions of stability of the solution. The symmetry preserving solution is stable everywhere except interior of the closed region shown by solid blue line. The stability of the symmetry breaking solution is shown by red, while the phase parity breaking solution is shown by gray. The parameters are $u = 0.01$, $\omega_0 = 1$, $\Gamma = 0.01$, $\lambda = -0.01$, $\phi_s = 1$, $\phi_a = 1.1$.

$$i\dot{a}_a = \lambda\omega_0\phi_s\phi_a(I_1 - I_2)a_s + [\omega_a + \lambda\omega_a\phi_a^2(I_1 + I_2)]a_a. \quad (52)$$

By presenting $a_s(t) = (A_s + \xi_s(t))e^{-i\omega t}$, $a_a(t) = (A_a + \xi_a(t))e^{-i\omega t}$ with A_s , A_a as the steady state obeying the stationary CMT equations (24) and $|\xi_s(t)| \ll |A_s|$, $|\xi_a(t)| \ll |A_a|$ we obtain the linearized time-dependent equations for complex ξ_s, ξ_a

$$\begin{pmatrix} Re(\dot{\xi}_s) \\ Im(\dot{\xi}_s) \\ Re(\dot{\xi}_a) \\ Im(\dot{\xi}_a) \end{pmatrix} = \hat{L} \begin{pmatrix} Re(\xi_s) \\ Im(\xi_s) \\ Re(\xi_a) \\ Im(\xi_a) \end{pmatrix}. \quad (53)$$

Their stability is determined by eigen values of the matrix \hat{L} which is time independent. The results of our calculation of stability are presented in Fig. 5 which shows that the stability of the phase parity breaking solution appears if only the defects are coupled and $\phi_s \neq \phi_a$. We collected the results of stability of all three solutions in Fig. 11 in the form of phase diagrams in plane of the incident wave amplitude and the frequency. One can see that the phase parity breaking solution is stable in some small area of the phase diagram.

E. Numerical calculations in photonic crystal

We numerically solve the Maxwell equations (1) for the TM mode in the PhC with defect nonlinear rods by expansion of electromagnetic field over maximally localized photonic Wannier functions [23, 24, 34]. The square lattice 2D PhC has the same parameters as given earlier [see Fig. 1(a)]. For the case of isolated linear defects with the same radius as the radius of host rods and the dielectric constant $\epsilon_d = 3$ their eigen frequency $\omega_0 = 0.3593$ in terms of $2\pi c/a$. Overlapping of the defect's monopole modes gives rise to splitting of this frequency $\omega_s = 0.3603, \omega_a = 0.3584$ as numerical computation of equations (1) gives. Respectively we obtain that the value of coupling $u = -0.001$. The corresponding bonding and anti-bonding modes for the nearest distance a between defects were found in Ref. [51]. For more distance $4a$ they are shown in Fig. 2. By the normalization condition (8) the heights of the amplitude modes at the defects equal $\phi_s = 0.5569$, $\phi_a = 0.6179$. Let us evaluate the dimensionless nonlinearity constant λ . We take in numerical calculations the incident power per length of order $100mW/a$ which corresponds to the incident intensity $I_0 = 100mW/a^2$. For chosen PhC lattice with period $a = 0.5\mu m$ we obtain that the incident intensity equals $0.04GW/cm^2$. With the use of $\epsilon = \epsilon_0 + 2\sqrt{\epsilon_0}n_2I_0$ we obtain

$$\lambda = -2\sqrt{\epsilon_0}n_2I_0. \quad (54)$$

We take the linear and nonlinear refractive indexes of the defect rods to be, respectively, $n_0 = \sqrt{\epsilon_0} = \sqrt{3}$, $n_2 = 2 \times 10^{-12}cm^2/W$. By substituting all of these estimates into (54) we obtain $\lambda \sim -0.9 \times 10^{-2}$ which is close to that used in the CMT consideration. Finally, we estimate the coupling of the defect mode with the propagation mode of

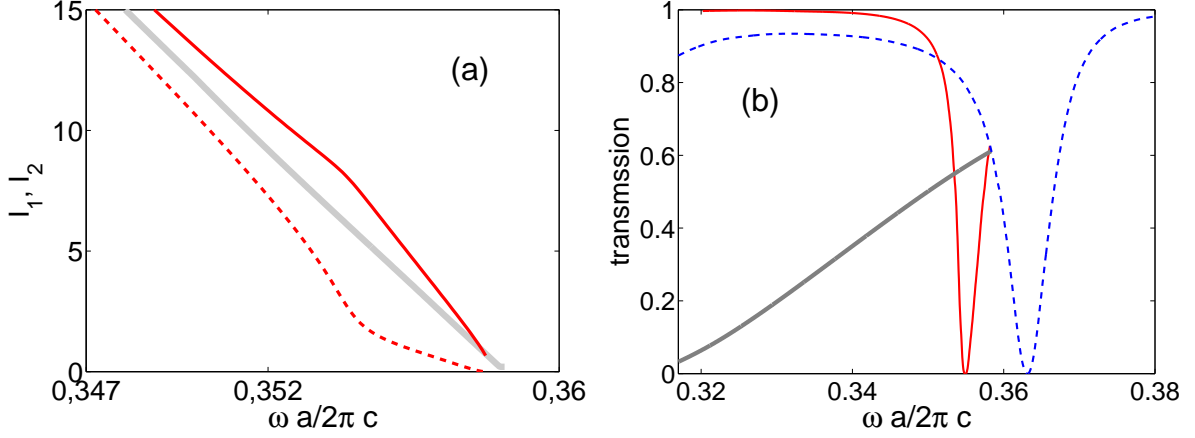


FIG. 12: Self-consistent solution for (a) the intensities of the EM field at the nonlinear defects and (b) transmission spectra in the PhC structure in the PhC structure shown in Fig. 1. The parameters of the PhC and defects are given in Fig. 2. The input power per length equals $100mW/a$. $n_2 = 2 \times 10^{-12}cm^2/W$, $\lambda = -0.009$.

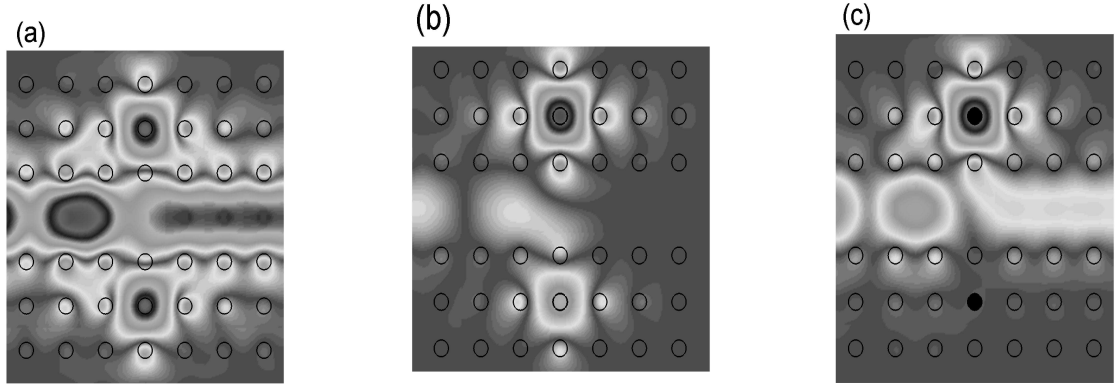


FIG. 13: Absolute value of the EM field solution for (a) the symmetry preserving solution $\omega a/2\pi c = 0.355$, (b) and (c) the symmetry breaking solution for $\omega a/2\pi c = 0.355$ and $\omega a/2\pi c = 0.358$ respectively. The EM wave incidents at the left of the waveguide.

the PhC waveguide $\sqrt{\Gamma}$. There are many ways to calculate Γ using for example Refs. [29, 52, 53]. In the present paper we estimated Γ numerically by using the following approach. We took the single linear defect aside the PC waveguide as shown in Fig. 1(a), and calculated the transmission spectra. By the resonance width of the spectra we evaluated $\Gamma = 0.00185$.

The self-consistent solutions are presented in the form of the intensities in Fig. 12(a), which are similar to the CMT results shown in Fig. 3(a). Also, one can see three solutions in the transmission shown in Fig. 12(b), as was found in the CMT model for the transmission shown in Fig. 5. Fig. 13 shows the EM field (the absolute value of the electric field) for the symmetry preserving solution (a) and for the symmetry breaking solution (b) and (c). In the latter case one can see that the field is strongly different at bottom and top. Moreover Figs. 3 and 12 show that there is a frequency at which the intensity of the EM field might be zero at the bottom defect. Indeed, Fig. 13(c) demonstrates this case.

In agreement with the model consideration Fig. 14 shows that current flows (the Poynting's vector patterns) are strongly different for the different solutions. For the symmetry preserving solution we have laminar current flow over the waveguide with excitation of two current vortices around each defect. The laminar flow over the waveguide and the vortical flows around defects are well separated. The whole current pattern is symmetrical relative to the symmetry transformation $y \rightarrow -y$. The picture has a similarity with ballistic electron transport in waveguide coupled to an off-channel quantum dot [54]. For the case of the symmetry breaking solution there is a current vortex inside the waveguide complemented by two vortices near each defect, as shown in Fig. 14 (b). The circulation in vortical flow around the upper defect is opposite to the circulation around the bottom defect. The vortical flow in the waveguide

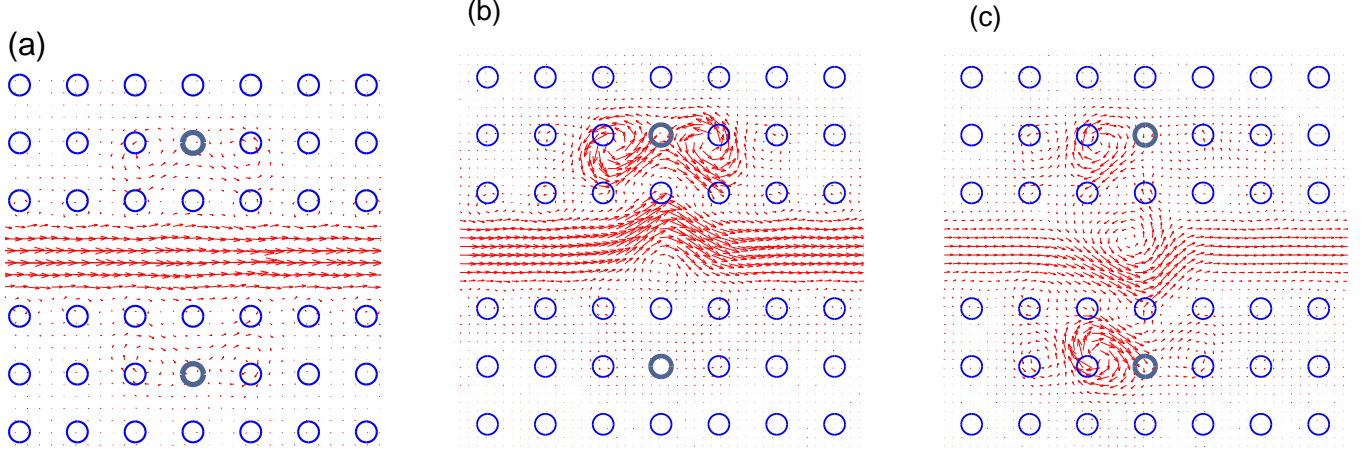


FIG. 14: Current flows for the symmetry preserving solution which inherits linear case (a), the symmetry breaking solution (b), and (c) the phase parity breaking one at $a\omega/2\pi c = 0.35$. Bold open circles mark the nonlinear defects.

and the vortical flows around the defects are well separated for both solutions. In the third case (c) for the phase parity breaking solution one can see the current vortex in the waveguide and single vortices around the defects are mixed. Nevertheless because of the continuity equation in the space beyond of the nonlinear defects $\nabla \cdot \vec{j}(x, y) = 0$ the vortical flows around the defects and in the waveguide can not cross.

IV. THE T-SHAPE WAVEGUIDE COUPLED WITH TWO NONLINEAR DEFECTS

One of the most ambitious goals in nonlinear optics is the design of an all-optical computer that will overcome the operation speeds in conventional (electronic) computers. Vital in this respect is the design of basic components such as all-optical routing switches and logic gates. It is believed that future integrated photonic circuits for ultra fast all-optical signal processing require different types of nonlinear functional elements such as switches, memory and logic devices. Therefore, both physics and designs of such all-optical devices have attracted significant research efforts during the last two decades, and most of these studies utilize the concepts of optical switching and bistability. One of the simplest bistable optical devices which can be built-up in photonic integrated circuits is a single cavity coupled with optical waveguide or waveguides [15, 55].

The concept of the all-optical switching is based on a discontinuous transition between the symmetry breaking solutions by a small change of the input [19]. Many of these devices employ a configuration of two parallel coupled nonlinear waveguides [18, 20, 56–58]. Recently Maes *et al* demonstrated the all-switching in the system of two nonlinear micro-cavities aligned along the waveguide [11] by the use of pulses of injected light. In the present section we use similar approach to demonstrate the all-switching effects in the T-shaped waveguide coupled with two nonlinear micro-cavities [59, 60].

We consider the PhC shown in Fig. 15 with the same parameters as given in Section III: the lattice constant $a = 0.5\mu m$, the cylindrical dielectric rods have radius $0.18a$ and dielectric constant $\epsilon = 11.56$. We substitute two defect rods of the same radius as shown in Fig. 15 made from an instantaneous Kerr media with the nonlinear refractive index $n = n_0 + n_2 I_0$ where $n_0 = \sqrt{3}$ and $n_2 = 2 \times 10^{-12} cm^2/W$. The corresponding equivalent configuration of the T-shaped waveguide with two nonlinear defects is presented in Fig. 16

We start with the position of the defect rods shown in Fig. 15 (a) which have strong coupling with the output waveguides 2 and 3, and negligibly weak coupling with the input waveguide 1. We consider a light given by the amplitude S_{1+} is incident into the waveguide 1 and outputs into all three terminals as shown schematically in Fig. 16. The outgoing amplitudes are labelled as S_{1-} , S_{2-} and S_{3-} . Each nonlinear optical cavity is assumed to be given by single mode amplitudes A_j , $j = 1, 2$ and coupled with the guides 2, 3 via the coupling constant γ shown in Fig. 16 by dotted lines and with the guide 1 via the coupling constant Γ .

We consider that the defects are not coupled. Therefore the eigen frequencies of the system of the defects equal the monopole eigen frequencies of the isolated defects $\omega_j = \omega_0 + \lambda |A_j|^2$, $j = 1, 2$ shifted because of the Kerr effect. Then

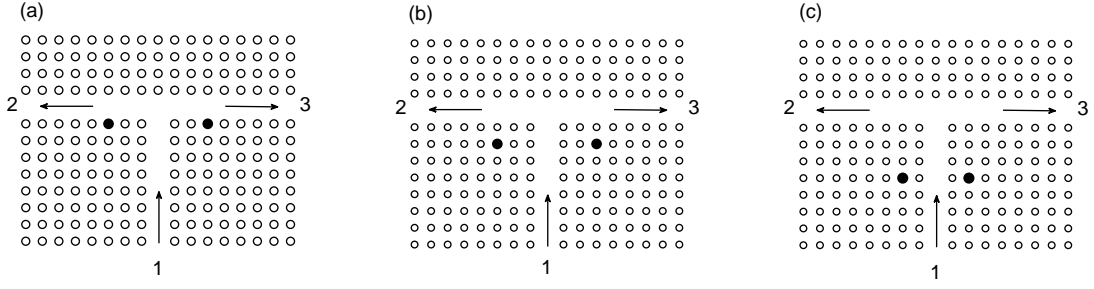


FIG. 15: T-shaped waveguide with two nonlinear defect rods. The cases (a)-(c) differ by the positions of the nonlinear defects.

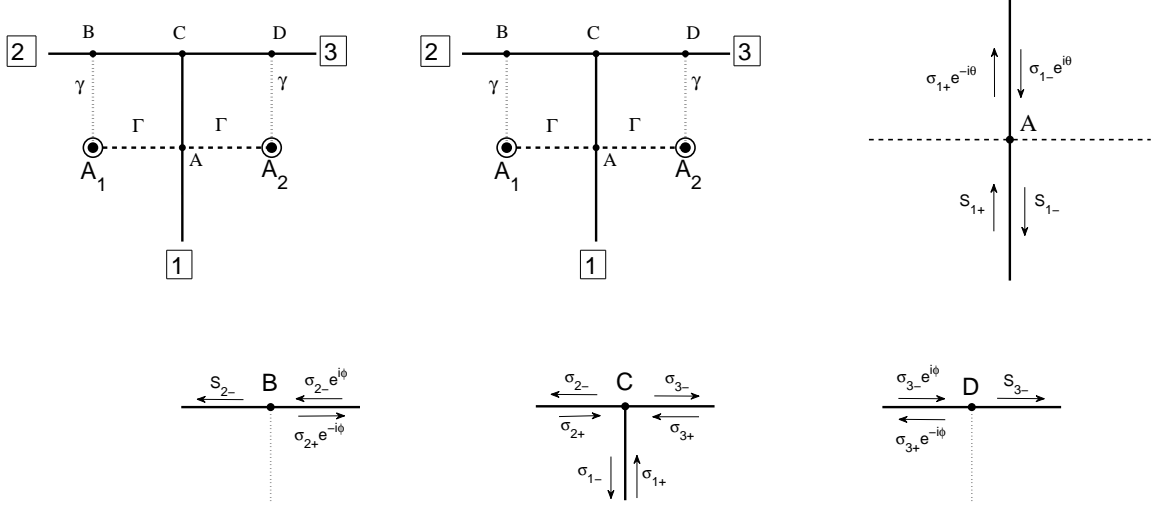


FIG. 16: CMT model of the T-shape photonic crystal waveguide coupled with two nonlinear defects shown by filled bold circles. The defects are coupled with input waveguide 1 via the constant Γ shown by dashed lines and with the output waveguides 2,3 via the constant γ shown by dotted line. Separately each connection is shown with corresponding light amplitudes.

the equations (17) will take the following form

$$\begin{aligned} (\omega - \omega_0 - \lambda|A_j|^2 + i\gamma + i\Gamma)A_1 + i\Gamma A_2 &= i\sqrt{\Gamma}(S_{1+} + \sigma_{1-}e^{i\theta}) + i\sqrt{\gamma}\sigma_{2-}e^{i\phi} \\ (\omega - \omega_2 + i\gamma + i\Gamma)A_2 + i\Gamma A_1 &= i\sqrt{\Gamma}(S_{1+} + i\sigma_{1-}e^{i\theta}) + i\sqrt{\gamma}\sigma_{3-}e^{i\phi} \end{aligned} \quad (55)$$

Here phases θ and ϕ as shown in Fig. 16 are the optical lengths through which light goes between the connections.

These equations are to be complemented by the equations for light amplitudes at each connection A, B, and D [33]

$$\begin{aligned} (\omega - \omega_1 + i\gamma + i\Gamma)A_1 + i\Gamma A_2 &= i\sqrt{\Gamma}(S_{1+} + \sigma_{1-}e^{i\theta}) + i\sqrt{\gamma}\sigma_{2-}e^{i\phi} \\ (\omega - \omega_2 + i\gamma + i\Gamma)A_2 + i\Gamma A_1 &= i\sqrt{\Gamma}(S_{1+} + i\sigma_{1-}e^{i\theta}) + i\sqrt{\gamma}\sigma_{3-}e^{i\phi}. \end{aligned} \quad (56)$$

These CMT equations are to be complemented by the equations for light amplitudes at each connection A, B, and D

$$\begin{aligned} \sigma_{1+}e^{-i\theta} &= S_{1+} - \sqrt{\Gamma}(A_1 + A_2) \\ S_{1-} &= \sigma_{1-}e^{i\theta} - \sqrt{\Gamma}(A_1 + A_2) \\ S_{2-} &= \sigma_{2-}e^{i\phi} - \sqrt{\gamma}A_1 \\ S_{3-} &= \sigma_{3-}e^{i\phi} - \sqrt{\gamma}A_2. \\ \sigma_{2+}e^{-i\phi} &= -\sqrt{\gamma}A_1. \\ \sigma_{3+}e^{-i\phi} &= -\sqrt{\gamma}A_2. \end{aligned} \quad (57)$$

TABLE I: Parameter sets of the CMT for PhC T-shaped waveguide shown in Fig. 15

Type of structure in Fig. 15	(a)	(b)	(c)
Γ (in terms of $a/2\pi c$)	0.0002	0.0002	0.00189
γ (in terms of $a/2\pi c$)	0.03093	0.00189	0.00002
ω_0 (in terms of $a/2\pi c$)	0.3609	0.365	0.3596

The T-connection at the C point connects ingoing and outgoing amplitudes by the S-matrix as follows

$$\begin{pmatrix} \sigma_{1-} \\ \sigma_{2-} \\ \sigma_{3-} \end{pmatrix} = \begin{pmatrix} a & b & b \\ b & c & d \\ b & d & c \end{pmatrix} \begin{pmatrix} \sigma_{1+} \\ \sigma_{2+} \\ \sigma_{3+} \end{pmatrix}. \quad (58)$$

In particular, the solution of the Maxwell equations for the T-shaped waveguide without defects gives the matrix elements of the S-matrix (58) $a = -0.3547 + 0.308i$, $b = 0.6 + 0.173i$, $c = -0.4319 + 0.2271i$, $d = -0.568 + 0.2225i$ at $\omega a/2\pi c = 0.35$. Eqs. (63), (57), and (58) form a full system of equations for 11 amplitudes $A_1, A_2, \sigma_{1+}, \sigma_{1-}, \sigma_{2+}, \sigma_{2-}, \sigma_{3+}, \sigma_{3-}, S_{1-}, S_{2-}, S_{3-}$. Substituting $S_{1+} = E_{in}e^{i\omega t}$, $A_{1,2} = A_{1,2}e^{-i\omega t}$ we obtain after some algebra the following stationary CMT equations

$$(\omega - H_{eff}) \begin{pmatrix} A_1 \\ A_2 \end{pmatrix} = iE_{in}F \begin{pmatrix} 1 \\ 1 \end{pmatrix}, \quad (59)$$

where

$$H_{eff} = \begin{pmatrix} \omega_1 - iG & -iH \\ -iH & \omega_2 - iG \end{pmatrix}, \quad (60)$$

$$\begin{aligned} G &= \gamma + \Gamma(1 + ae^{2i\theta}) + \gamma de^{2i\phi} + \sqrt{\gamma\Gamma}(b+c)e^{i\theta+i\phi}, \\ H &= \Gamma + \sqrt{\gamma\Gamma}(b+c)e^{i\theta+i\phi} + \Gamma ae^{2i\theta} + \gamma de^{2i\phi}, \\ F &= \sqrt{\Gamma}(1 + ae^{2i\theta}) + \sqrt{\gamma b}e^{i(\theta+\phi)}. \end{aligned} \quad (61)$$

We can calculate all parameters which are necessary in Eqs. (59), (60), and (61). For the light transmission in straight waveguide coupled with the single linear off-channel defect positioned at different positions we able to extract the coupling constant of the cavity with PhC waveguide Γ and the eigen frequency of monopole mode ω_0 . The results are collected in Table I. The limiting case of the T-shaped waveguide with $\Gamma = 0$ is considered in Ref. [59] with results qualitatively close to those shown in Fig. 19. Here we find the solutions with the substitution of concrete parameters listed in Table I and present the output light transmission to the left and to the right waveguides. We start with the case shown in Fig. 15 (a).

Moreover we present real dispersion curve $\omega(k)$ calculated for the straight PhC waveguide to find as the optical length given by the phase θ or ϕ depends on the frequency ω . This curve is shown in Fig. 17 by solid curve for the parameters of PhC given in Fig. 1. In the vicinity of the BSC frequency $\omega_c a/2\pi c = 0.3402$ we approximate the dispersion curve as linear to obtain

$$\frac{phase}{\pi} = 1 + \frac{17.68(\omega - \omega_c)a}{2\pi c}. \quad (62)$$

parameters for the phases.

The case of the T-shaped structure shown in Fig. 15(a) has an analogy with the Fabry-Pérot interferometer (FPI) comprising two off-channel nonlinear cavities. As was shown in Ref. [22] there is a series of the self-induced BSCs which are the standing waves between the off-channel cavities. It was shown that the BSCs exist for any distance between the off-channel defect rods because of their nonlinearity [22]. Similar BSC solutions are expected to exist in the present case of the T-shaped waveguide coupled with two off-channel cavities shown in Fig. 15(a). However these solutions must be the standing waves with nodes at the point of connection of the waveguides. Therefore in the present case the BSCs are the anti-symmetric standing waves. Fig. 18 shows one of these waves in the T-shaped waveguide with two nonlinear defect rods with the eigen frequency $\omega_c a/2\pi c = 0.3402$ which satisfies the condition $3k(\omega_c)a = \pi$.

For the linear case the BSC has zero coupling with the symmetric EM wave which inputs in the waveguide 1. However as was considered in section II nonlinearity gives rise to the important effect of the excitation of BSC by

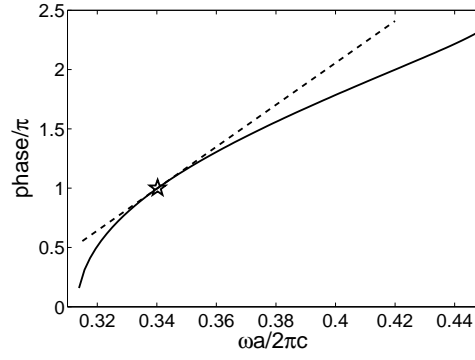


FIG. 17: Frequency behavior of the optical length (phase) shown by solid line for the straight PhC waveguide which is fabricated by removing one row of dielectric rods. The parameters of the PhC are listed in figure caption of Fig. 1. The BSC point is marked by star.

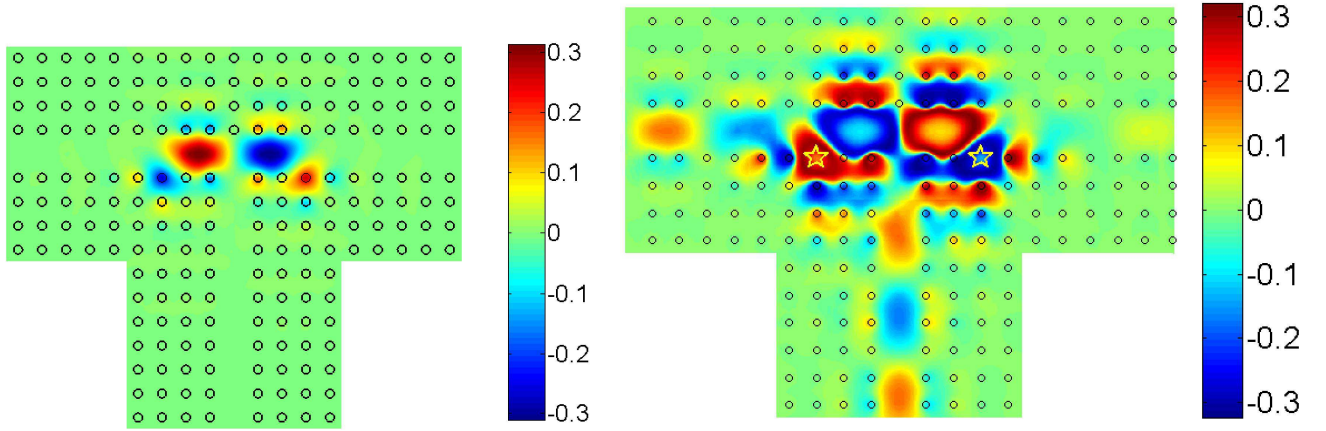


FIG. 18: Solutions of Maxwell equations for the case shown in Fig. 15 which demonstrate (a) the anti-symmetric FPI BSC (anti-symmetric standing wave between nonlinear off-channel defects marked by stars) with frequency $\omega_c a/2\pi c = 0.3402$ for zero input power $P = 0$ and (b) as this BSC mixes with incident EM wave to give rise to the symmetry breaking because of nonlinearity for $P = 1.94W/a$. Yellow stars mark defect rods.

the transmitted wave, (i.e., an interaction between the anti-symmetric BSC and the symmetric transmitted wave). As a result the total solution lacks the mirror symmetry of the PhC structure shown in Fig. 15. That is one of the scenarios of the symmetry breaking. Note, that Maes *et al.* [11] have already reported the symmetry breaking in the FPI. In order for the FPI with two off-channel nonlinear cavities to have the mirror symmetry equal input power must be applied to both sides of the FPI [11]. In our case of the T-shaped waveguide this symmetry is achieved by application of the input power via the additional waveguide positioned at the center of the FPI.

Figure 19(a) demonstrates the solution for the light intensities of the cavities $I_j = c|E_j|^2/8\pi$, $j = 1, 2$ with broken mirror symmetry where E_j are the amplitudes of the electric field in thin defect rods for two values of input power. The solution converges to the BSC point marked by the star if the input power limits to zero. At this point the symmetry is restored. As a result for the input power $P \neq 0$ the light transmission from the input waveguide 1 to the left waveguide 2 differs from the transmission and to the right waveguide 3 as seen from Fig. 19(b). Moreover the difference $T_L - T_R$ crucially depends on the frequency in the vicinity of the BSC point. Figure ?? demonstrates the solution of the Maxwell equations for the z -component of electric field (the scattering wave function) breaks the mirror symmetry because of mixing the symmetric input wave with the anti-symmetric BSC as shown in Fig. 18(b). The intensity of the defect's modes is centered around the BSC intensity which is rather large as shown in Fig. 19(a) while the incident light intensity $P \sim 1 \cdot W/a$. Thereby we have chosen exponential scaling for the solution of the Maxwell equations presented in Fig. 18(b) in order to distinguish waves in waveguides.

As was shown in the framework of the CMT there might appear an additional branch of a loop shape for the

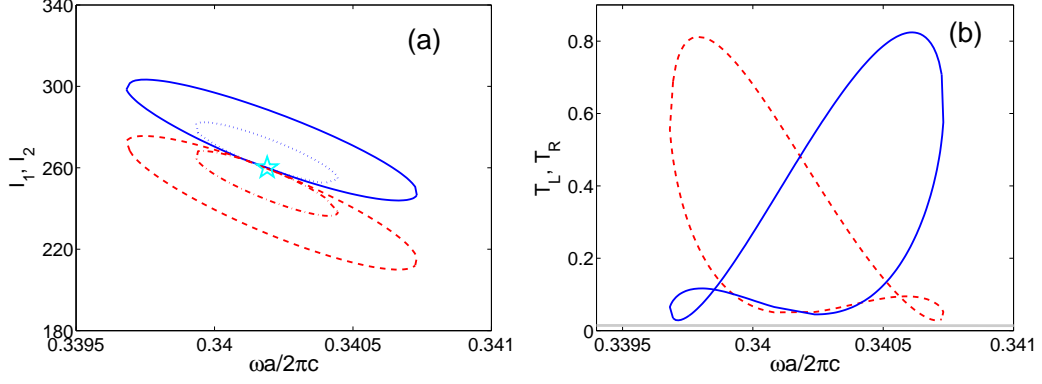


FIG. 19: (a) Frequency behavior of light intensities at the defect rods given in terms of W/a^2 . Dotted blue and dash-dotted red lines correspond to the input power equal to $0.48W/a$, solid blue and dashed red lines do to $1.92W/a$. Only those solution for intensities is shown which breaks the symmetry. (b) The frequency dependence of the transmissions to the left T_L (blue solid lines) and to the right T_R (red dashed lines) for the PhC T-shaped waveguide shown in Fig. 15 (a). The BSC point is shown by blue star.

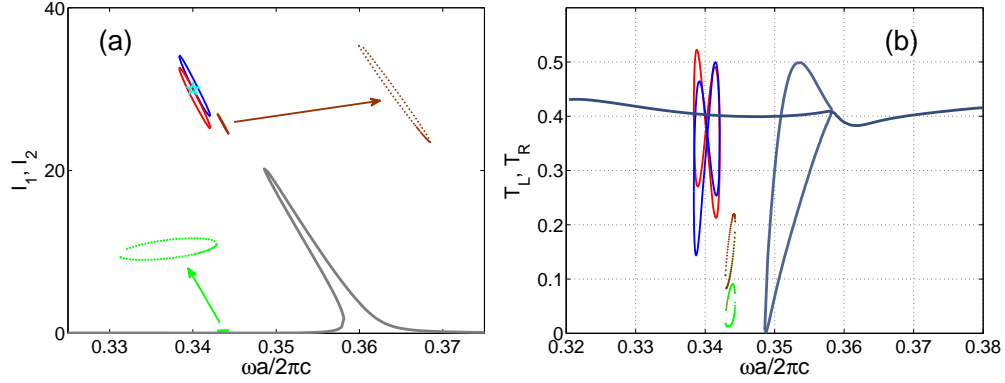


FIG. 20: Frequency behavior of (a) the light intensities at the defect rods (in terms of $I_0 = W/a^2$) and (b) transmissions T_L and T_R for the PhC T-shaped waveguide shown in Fig. 15 (b). The input power equals $5.57W/a$. The symmetric solution is shown by solid gray line which inherits the linear case. The symmetry breaking solution because of the mixing the symmetric transport solution with the anti-symmetric BSC is shown by solid blue and red lines. The next symmetry breaking solution because of a bistability of the transmission in each output waveguides is shown by dotted brown and green lines. Zooming of loops are shown by arrows in (a).

symmetry breaking solution with growth of the input power [59]. The numerical results for the solution of the Maxwell equations completely agree with these model results as seen from Fig. 20(a) by dotted brown and green lines. The loops shown by dotted lines in Fig. 20 are the result of individual instability that arises for transmission in the left or right waveguide coupled with the left or right nonlinear off-channel cavity [59]. Loops in the intensities are reflected in the loops in the transmission to the left and for the transmission to the right as shown in Fig. 20(b) by dotted brown and green lines respectively.

Bistability of the light transmission in the PhC waveguide coupled with nonlinear optical cavity crucially depends on the coupling: the smaller a coupling the less input power is needed for bistability [15]. For case (a) in Fig. 15 the coupling is rather large to observe bistability in the transmission. However case (b) has the sufficiently smaller coupling as one can see from Table I. As a result case in Fig. 15(b) gives rise to additional loops as shown in Fig. 20 for larger input power $5.57W/a$. Figure 21 shows the wave function for the symmetry preserving solution (a) and the symmetry breaking solution (b) and (c). Cases (b) and (c) differ by the frequency. One can see from Fig. 21(a) and Fig. 21(b) that for the symmetric solution the transmission excites the cavities weakly, while for the symmetry breaking solution the defects are strongly excited because of mixing the injecting symmetrical wave with the anti-symmetrical FPI BSC. Figure 21(c) shows that for the frequency in the loop domain $\omega a/2\pi c = 0.3442$ the first nonlinear cavity is excited much more than the second one that is correlated with the outputs.

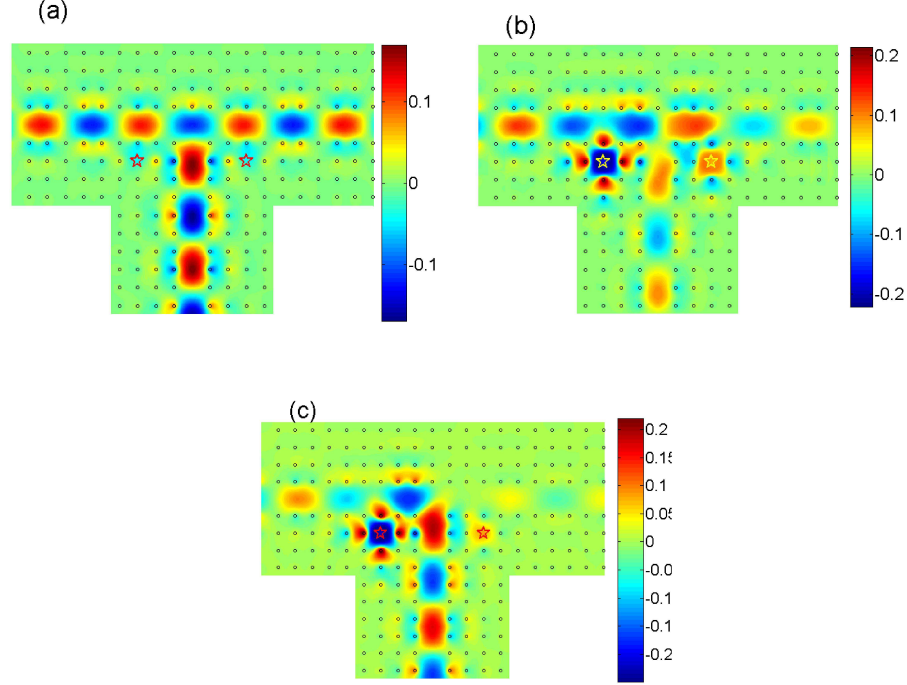


FIG. 21: The EM field solution in a scale $real(E_z) \exp(-|E_z|)$ for (a) the symmetry preserving solution for $\omega a/2\pi c = 0.3442$, (b) the symmetry breaking solution caused by the BSC for $\omega a/2\pi c = 0.3388$, and (c) the for $\omega a/2\pi c = 0.3442$. Yellow stars mark defect rods.

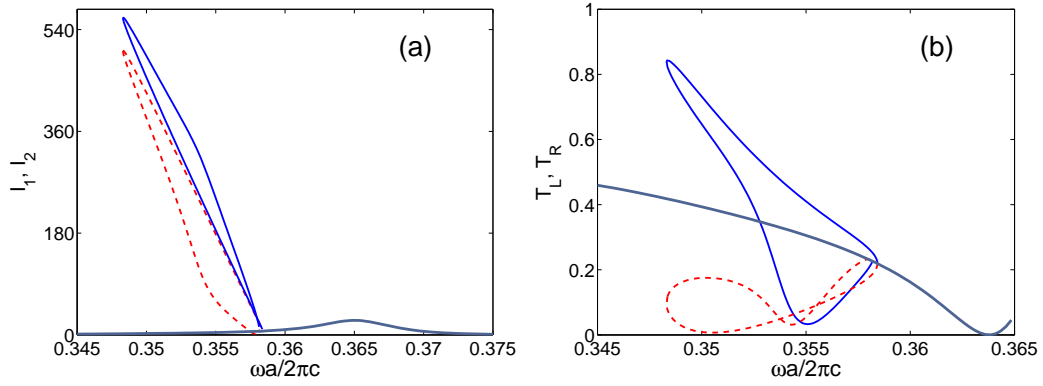


FIG. 22: Frequency behavior of (a) the light intensities at the defect rods and (b) transmissions T_L and T_R for the PhC T-shaped waveguide shown in Fig. 15(c). The input power $P = 0.48W/a$. Only those solution is shown in (b) which demonstrates different outputs in the left (red dashed line) and right (blue solid line) waveguides.

The T-shaped waveguide coupled with two nonlinear cavities shown in Fig. 15 is remarkable in that it allows the limit to the FPI [case (a)] with the FPI BSC in the form of the standing waves between two off-channel defects [22] as well as the limit to case (c) in Fig. 15 with the BSC in the form of the anti-bonding defect's state. Patterns of such anti-bonding BSC in PhC straight waveguide coupled with two cavities positioned perpendicular to the waveguide are shown in Fig. 2.

The nonlinearity gives rise to mixing the anti-bonding BSC with the wave transmitted over waveguide 1. For the linear defect rods this state would be the perfect BSC. For the nonlinear cavities mixing this anti-bonding BSC with symmetric input light leads to the breaking of the mirror symmetry to give rise to the breaking of symmetry in the input waveguide. Then for the evolution of this structure to the T-shaped case can expect different outputs to the

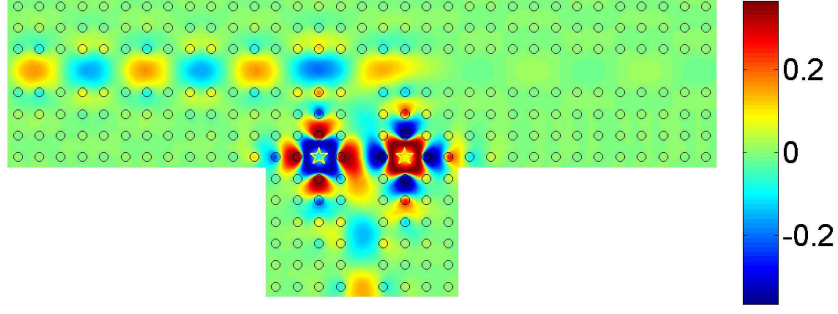


FIG. 23: EM field for the symmetry breaking solution $\omega a/2\pi c = 0.3505$. Light is incident into the 1 waveguide and scatters to the left and right waveguides 2 and 3. $P = 0.48W/a$.

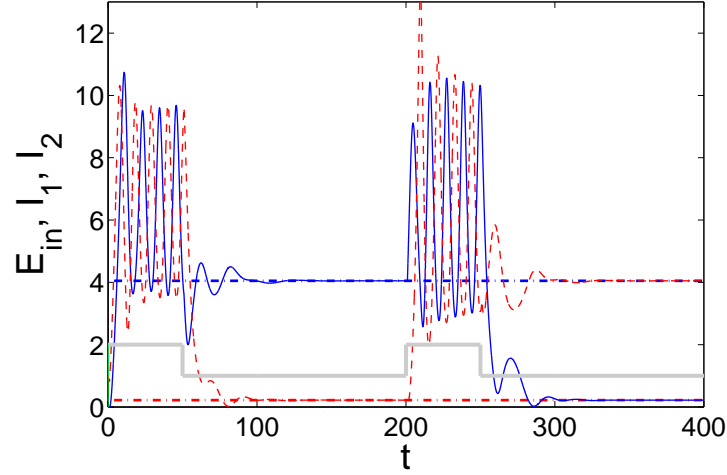


FIG. 24: The time dependence of the amplitudes of the light amplitudes $|A_1|, |A_2|$ in the cavities (solid and dashed respectively) which follow the impulses of the input amplitude E_{in} (gray). We take the cavities oscillate in non symmetric way: $A_1 = 0, A_2 = 1$.

right and to the left. Indeed, in spite of the small difference of the defect intensities presented in Fig. 22(a) the transmissions T_L and T_R demonstrate vast difference including the case of almost perfect blocking of the transmission to the left as shown in Fig. 22(b) for $\omega a/2\pi c = 0.3505$. Figure 23 shows the anti-bonding BSC is mixed to the transport over the input waveguide to give rise to the symmetry breaking solution.

These results are extremely important for the switching of the output power from the left waveguide to the right one. In order to switch the system from one asymmetric state to the other we following Refs. [11, 13] apply pulses of the input power injected into the waveguide 1. The direct numerical solution of the temporal CMT equation

$$\begin{aligned} i\dot{A}_1 &= (\omega_1 - i\gamma)A_1 + i\sqrt{\gamma}\sigma_2 e^{i\phi} \\ i\dot{A}_2 &= (\omega_2 - i\gamma)A_2 + i\sqrt{\gamma}\sigma_3 e^{i\phi} \end{aligned} \quad (63)$$

with $S_{1+}(t) = E_{in}(t)e^{-i\omega t}$ is shown in Fig. 24 which demonstrates the switching effect. The stepwise time behavior of amplitude $E_{in}(t)$ is shown by gray line. One can see that after the first impulse of the input amplitude the oscillations of the cavity amplitude relax onto the stable stationary solutions with broken symmetry. Moreover after each next impulse the state of the system transmits from one asymmetric state to the other as was observed by Maes *et al* [11].

V. DIPOLE MODES OF THE SINGLE NONLINEAR DEFECT COUPLED WITH WAVEGUIDE

If to present the defect by the single monopole mode $E_s(\mathbf{x})$ we obtain from Eqs. (17)

$$[\omega - \omega_s - \lambda|A_s|^2 - i\Gamma_s]A_s = i\sqrt{\Gamma_s}E_{in}, \quad (64)$$

$$t = E_{in} - \sqrt{\Gamma_s} A_s, \quad (65)$$

where $\lambda = -\frac{3}{4}\sigma\chi^{(3)}(\omega_s)E_s((\mathbf{x}_d)^2)$. That model has attracted interest over the past two decades because of analytical treatment and its generality for description of bistability phenomena [15, 37–43]. However the monopole eigenfunction presents only the trivial identical symmetry transformation. Respectively there is no room for the breaking of symmetry.

In this respect the system becomes nontrivial if we include two eigen dipole modes $E_1(\mathbf{x})$ and $E_2(\mathbf{x})$ of the defect rod with the eigen-frequencies ω_1 and ω_2 . The modes are shown in Fig. 25. Respectively, the electric field at the thin

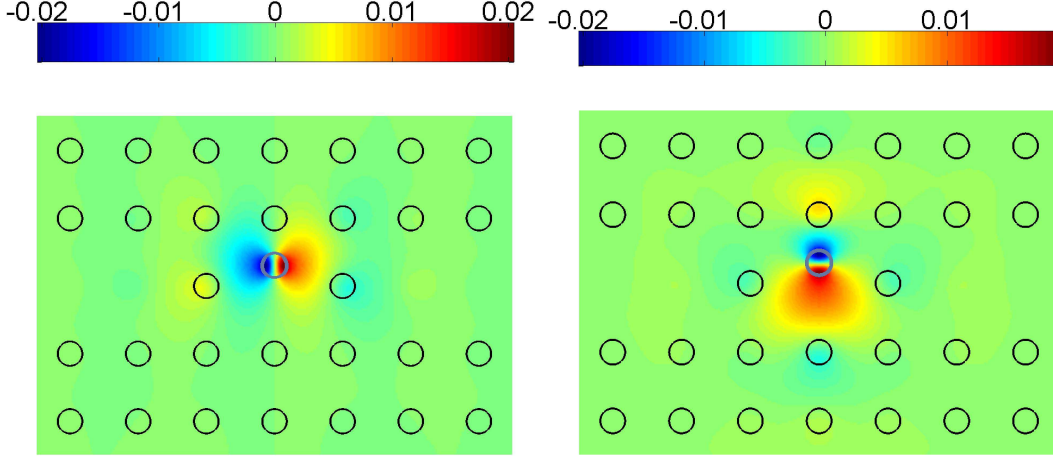


FIG. 25: Two defect dipole eigen-modes with the eigen frequencies $\omega_1 = 0.3578\pi a/c$ and $\omega_2 = 0.3616\pi a/c$ in the two-dimensional square lattice PhC consisted of the GaAs dielectric rods with radius $0.18a$ and dielectric constant $\epsilon = 11.56$ where $a = 0.5\mu m$ is the lattice unit. These rods are shown by black open circles. The defect shown by open gray circle has the same radius $0.18a$ and $\epsilon_0 = 30$. Its center is positioned at $x_d = 0, y_d = 0.3a$.

defects can be expanded over these dipole modes $E(\mathbf{x}_d) = A_1 E_1(\mathbf{x}_d) + A_2 E_2(\mathbf{x}_d)$ only. Substituting that expansion into Eq. (16) we obtain that Eq. (17) will take the following form

$$\begin{aligned} [\omega - \omega_1 - \lambda_{11}|A_1|^2 - \lambda_{12}|A_2|^2 + i\Gamma_1]A_1 - 2\lambda_{12}Re(A_1^* A_2)A_2 &= i\sqrt{\Gamma_1}(S_1^+ - S_2^+), \\ -2\lambda_{12}Re(A_1^* A_2) + [\omega - \omega_1 - \lambda_{22}|A_2|^2 - \lambda_{12}|A_1|^2 + i\Gamma_2]A_2 &= i\sqrt{\Gamma_2}(S_1^+ + S_2^+), \end{aligned} \quad (66)$$

where $S_{1,2}^+$ are the amplitudes of light injected simultaneously into both sides of the waveguide. Here with accordance to Eq. (14) we have

$$\lambda_{mn} = \frac{3}{16\epsilon^{3/2}}\chi^{(3)}(\omega_m + \omega_n)Q_{mn}, \quad Q_{mn} = \int E_m^2(\mathbf{x})E_n^2(\mathbf{x})d^2\mathbf{x}. \quad (67)$$

Moreover we have taken into account the symmetry relations for the coupling constants of the dipole modes with the waveguide solutions [66]. As seen from Fig. 25 the first dipole mode has the coupling with the left and the right ingoing waves opposite signs while the second dipole mode has the same coupling with these waves. Therefore the coupling matrix in Eq. (18) equals

$$W = \begin{pmatrix} \sqrt{\Gamma_1} & -\sqrt{\Gamma_1} \\ \sqrt{\Gamma_2} & \sqrt{\Gamma_2} \end{pmatrix}. \quad (68)$$

Moreover Eq. (66) must be complemented by equation for the transmission amplitude

$$\begin{aligned} t_{LR} &= S_1^+ - i\sqrt{\Gamma_1}A_1 + i\sqrt{\Gamma_2}A_2, \\ t_{RL} &= S_2^+ - i\sqrt{\Gamma_1}A_1 + i\sqrt{\Gamma_2}A_2. \end{aligned} \quad (69)$$

Fig. 26 shows the self-consistent solutions of Eq. (66) after substitution of the following model parameters $\omega_1 = 0, \omega_2 = 0.01, \lambda_{11} = \lambda_{22} = 0.1, \lambda_{12} = 0.05, \Gamma_1 = 0.1, \Gamma_2 = 0.03$. One can see that for the symmetry preserving branch

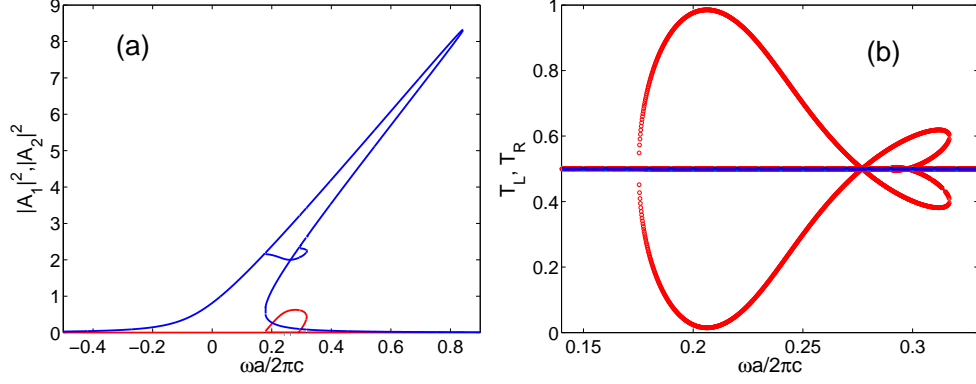


FIG. 26: Frequency behavior of (a) intensities of dipole modes and (b) transmissions to the left $T_L = |t_{RL}|^2$ and to the right $T_R = |t_{LR}|^2$ for light injection $S_{1,2}^+ = 0.025$ onto both sides of the straight forward waveguide. Blue lines show the intensity of even dipole mode, while red lines show the intensity of odd dipole mode. The model parameters are listed in the text.

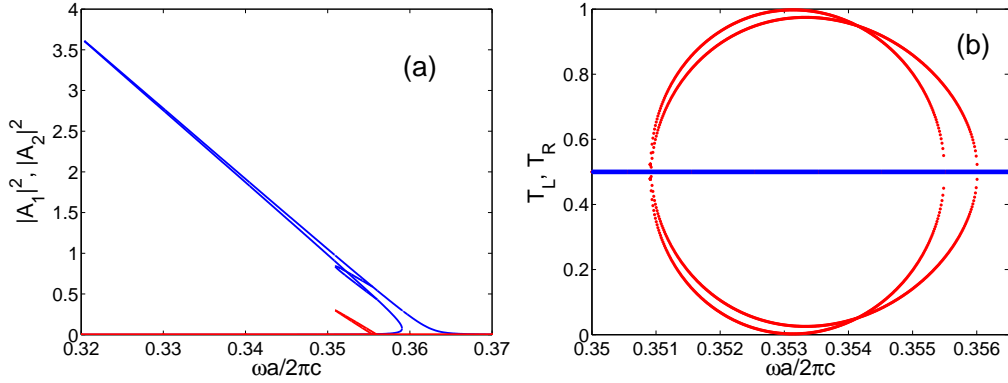


FIG. 27: Frequency behavior of (a) intensities of dipole modes and (b) transmissions to the left and to the right in real 2D PhC for $S_{1,2} = 0.015$. Dash blue line shows the symmetry preserving solution, solid red line shows the symmetry breaking solution, and grey thick line shows the phase parity breaking solution.

the first even dipole mode is excited with frequency behavior typical for the single nonlinear mode described by Eq. (36) while the second odd dipole mode is not excited because of symmetry. Respectively, the transmission probability to both sides of the waveguide equals $1/2$ because of normalization condition for the intensity of input light and unitarity of the S-matrix $|S_1|^2 + |S_2|^2 + |t_{LR}|^2 + |t_{RL}|^2 = 1$. However there is also the symmetry breaking branch in some narrow frequency domain. Respectively, that branch gives rise to an asymmetry in the light outputs. Moreover there is a frequency at which the right (left) output is blocked almost perfectly.

Also we consider the phenomenon of the symmetry breaking based on the parameters calculated in the 2D square lattice PhC with parameters given earlier. The results for the eigen frequencies are collected in Fig. 25 caption where the parameters of the PhC are given too. The coupling constants are the following $\Gamma_1 = 0.00075$, $\Gamma_2 = 0.00025$ in terms of $2\pi c/a$. In order to enhance the coupling constants we substituted two additional linear rods nearby the nonlinear defect rod as shown in Fig. 25. Let us evaluate the nonlinearity constants λ_{mn} . With use $\epsilon_d = \epsilon_0 + 2\sqrt{\epsilon_0}n_2I_0$, $n_2 \approx \frac{2\pi\chi^{(3)}}{n_0}$ we obtain from (70)

$$\lambda_{mn} = -\frac{3\pi}{8}\sqrt{\epsilon_0}n_2I_0 \int E_m^2(\mathbf{x})E_n^2(\mathbf{x})d^2\mathbf{x}. \quad (70)$$

We take the linear and nonlinear refractive indexes of the defect rods are, respectively, $n_0 = \sqrt{\epsilon_0} = \sqrt{3}$, $I_0 = 1.8W/a$, $n_2 = 2 \times 10^{-12} \text{cm}^2/\text{W}$ [63, 64]. Moreover substituting the dipole modes into integrals in Eq. (70) we obtain $Q_{11} = 0.0123$, $Q_{22} = 0.0114$, $Q_{12} = 0.0037$. Results of solution of the self-consistency equations for two complex amplitudes A_1 and A_2 are presented in Fig. 27(a). Correspondingly from Eq. (69) we obtain the transmission

coefficients shown in Fig. 27(b).

VI. SUMMARY AND CONCLUSIONS

As by direct solution of the Maxwell equations as well as by solution of the CMT equations we have demonstrated the symmetry breaking in the system of two nonlinear defects coupled with waveguide through which a light is injected. The defects are aligned symmetrically relative to the waveguide as shown in Fig. 1, so there is an inversion symmetry relative to the waveguide axis. The thin dielectric rods made from Kerr media are these defects which presented by the eigen monopole mode whose eigen frequency belongs to the propagation band of the waveguide. We assume that other eigen modes are beyond the band, and therefore have no coupling with the injected light with accuracy of evanescent modes.

That simplest system is remarkable in that it reveals as nonlinearity gives rise to the breaking of symmetry. Indeed, let us take temporarily the defects are linear. If the coupled defects were isolated, it would have only two eigenmodes, bonding (even) and anti-bonding (odd) with corresponding eigen frequencies (21). For light propagating over the waveguide we take that the solution is symmetrical relative to the inversion. Then the light can excite only the bonding mode A_s to give rise typical resonance dip at the symmetrical eigen frequency ω_s while the anti-bonding mode A_a would remain hidden for the propagating light. Obviously, that mode is the simplest case of the bound state in continuum [16, 67, 68]. That state can be superposed to the scattering function with coefficient determined by a way to excite the anti-bonding mode [47]. However the principle of linear superposition is not correct in the nonlinear case. Therefore the nonlinearity gives rise to interaction of the scattering state with the anti-bonding mode, i.e., to the interaction of the symmetric propagating light with the anti-bonding mode. That obviously breaks the inversion symmetry as explicitly shown in Figs. 13(b), 13(c), 20(b), and 20(c). Obviously, the mixing gives total state which is nor symmetrical neither anti symmetrical, breaking the mirror symmetry. Further we have shown that the symmetry can be broken not only because of different light intensities but also because of different phases of light oscillations at the cavities to provoke the Josephson like current between cavities [17]. For the light transmission in two-dimensional PhC the Poynting power current is an analog of the Josephson current, which is shown in Fig. 14(c). It is clear that for the light transmission in PhC waveguide there is the power current over the waveguide. However if the waveguide is coupled with nonlinear defects the current pattern might be rather complicated even in the symmetry preserving scenario as shown in Fig. 14(a). One can see that laminar current flow over the waveguide induces two vortices around the defects which obey the mirror symmetry. As the symmetry has broken the vortex in the waveguide appears which is well separated from the defect vortices. Although the mirror symmetry relative to circulation of currents in defect vortices is broken, however, the symmetry is remained relative to absolute value of current flows. At last, for the phase parity breaking solution still there is symmetry in absolute value of current, but all vortices are exchanging by current flows as seen from Fig. 14(c).

The T-shaped waveguide coupled with two symmetrically positioned nonlinear defects as shown in Fig. 15 can be considered as a combination of the previous system and the Fabry-Pérot interferometer (FPI) consisted of two nonlinear off-channel cavities aligned along the straightforward waveguide considered in Refs. [11, 12, 22]. As was shown in Ref. [22] there is a discrete set of the a self-induced bound states in continuum (BSC) which are standing waves between off-channel cavities which are to be anti-symmetric in order to elucidate an escape to the input waveguide 1. As dependent on position of the nonlinear defects shown consequently in Fig. 15 the system goes from the FPI (case a) to the system considered in section II (case c). In the case (a) the nonlinearity couples the FPI BSC shown in Fig. 18 with the incident wave which is symmetrical relative to the inversion left to right. As the result the inversion symmetry breaks as shown for real PhC in Figs. 21(b) and 21(c) to give rise to strong asymmetry of light outputs to the left and to the right as shown in Fig. 22(b). Similarly, the nonlinearity mixes the anti-bonding hidden state with the symmetric incident wave as shown in Fig. 23 to give rise different outputs too. At last, for the nonlinear defects are coupled as with input waveguide as well as with output waveguides the frequency behavior of the transmissions is complicated as shown in Fig. 22(b). In Ref. [59] we demonstrate as these phenomena can be explored for all-optical switching of light transmission from the left output waveguide to the right one by application input pulses.

In section V we show that breaking of symmetry might occur even for the single nonlinear defect positioned in the straight forward waveguide provided that the defect is presented by two dipole modes. That model embraces two degrees of freedom of the defect while in the former models each defect was presented by the only degree of freedom.

Acknowledgments

AS is grateful to Boris Malomed for fruitful and helpful discussions. The work is partially supported by RFBR

grant 12-02-00483.

-
- [1] E.A. Ostrovskaya, Y.S. Kivshar, M. Lisak, B. Hall, F. Cattani, and D. Anderson, Phys.Rev. **A61**, 031601 (2000); R.D. Agosta, B.A. Malomed, and C. Presilla, Phys.Lett. **A275**, 424 (2000).
 - [2] N. Akhmediev and A. Ankiewicz, Phys. Rev. Lett. **70**, 2395 (1993).
 - [3] R. Tasgal and B.A. Malomed, Physica Scripta, **60**, 418 (1999).
 - [4] A. Gubeskys and B.A. Malomed, Eur. Phys. J. **D28**, 283 (2004).
 - [5] V.A. Brazhnyi and B.A. Malomed, Phys. Rev. **A83**, 053844 (2011).
 - [6] M. Haelterman and P. Mandel, Opt. Lett., **15**, 1412 (1990).
 - [7] T. Peschel, U. Peschel, and F. Lederer, Phys. Rev. A **50**, 5153 (1994).
 - [8] I.V. Babushkin, Yu.A. Logvin, and N.A. Loiko, Quant. Electronics, **28**, 104 (1998).
 - [9] J.P. Torres, J. Boyce, and R.Y. Chiao, Phys. Rev. Lett. **83**, 4293 (1999).
 - [10] L. Longchambon, N. Treps, T. Coudreau, J. Laurat, and C. Fabre, Opt. Lett. **30**, 284 (2005).
 - [11] B. Maes, M. Soljačić, J.D. Joannopoulos, P. Bienstman, R. Baets, S-P. Gorza and M. Haelterman, Opt. Express, **14**, 10678 (2006).
 - [12] B. Maes, P. Bienstman, and R. Baets, Opt. Express, **16**, 3069 (2008).
 - [13] K. Otsuka, K. Ikeda, Opt. Lett., **12**, 599 (1987).
 - [14] K. Huybrechts, G. Morthier, and B. Maes, J. Opt. Soc. Am. B **27**, 708 (2010).
 - [15] J. Joannopoulos, S.G. Johnson, J.N. Winn and R.D. Meade, *Photonic Crystals: molding the flow of light* (Princeton University Press, Princeton, N Y, 2008)
 - [16] E.N. Bulgakov, K.N. Pichugin, and A.F. Sadreev, Phys. Rev. B **83**, 045109 (2011).
 - [17] E.N. Bulgakov, K.N. Pichugin, and A.F. Sadreev, J. Phys.: Condens. Mat., **23**, 065304 (2011).
 - [18] S. M. Jensen, *The nonlinear coherent coupler*, IEEE J. Quantum Electron. **QE-18**, 1580 (1982).
 - [19] A.A. Maier, Sov. J. Quantum Electron. **12**, 1940 (1982).
 - [20] S. R. Friberg, Y. Silberberg, M. K. Oliver, M. J. Andrejco, M. A. Saifi, and P. W. Smith, , Appl. Phys. Lett. **52**, 1135 (1987).
 - [21] H.M. Gibbs, *Optical Bistability: Controlling Light with Light* (Academic,1985).
 - [22] E.N. Bulgakov and A.F. Sadreev Phys. Rev.B **81**, 115128 (2010).
 - [23] N.Marzari and D.Vanderbilt, Phys.Rev. **B56**, 12847 (1997).
 - [24] K. Busch, S.F. Mingaleev, A. Garcia-Martin, M. Schillinger, and D. Hermann, J. Phys. : Cond. Mat. **15**, R1233 (2003).
 - [25] L.D. Landau, E.M. Lifzhits, *Electrodynamics of continuous media* (Pergamon, Oxford, 1980).
 - [26] J. Bravo-Abad, S. Fan, S.G. Johnson, J.D. Joannopoulos, and M. Soljačić, J. Lightwave Technol. **25**, 2539 (2007).
 - [27] M. Skorobogatiy and J. Yang, *Fundamentals of Photonic Crystal Guiding* (Cambridge, Univ. Press, 2009).
 - [28] J.N. Winn, S. Fan, J.D. Joannopoulos, and E.P. Ippen, Phys. Rev. **B59**, 1551 (1999).
 - [29] A. R. Cowan and J.F. Young, Phys. Rev. E **68**, 046606 (2003).
 - [30] H.A.Haus, *Waves and Fields in Optoelectronics* (Prentice-Hall, N.Y., 1984).
 - [31] C. Manolatou, M. J. Khan, S. Fan, P. R. Villeneuve, H. A. Haus, and J. D. Joannopoulos, IEEE J. Quantum Electron. **35**, 1322 (1999).
 - [32] S. Fan, W. Suh, and J.D. Joannopoulos, J. Opt. Soc. Am. **A20**, 569 (2003).
 - [33] W. Suh, Z. Wang, and S. Fan, IEEE J. of Quantum Electronics, **40**, 1511 (2004).
 - [34] E.N. Bulgakov and A.F. Sadreev, Phys. Rev. **B78**, 075105 (2008).
 - [35] S. Fan, P.R. Villeneuve, J. D. Joannopoulos, M. J. Khan, C. Manolatou, and H. A. Haus, Phys. Rev. **B59**, 15 882 (1999).
 - [36] P.R. Villeneuve, S. Fan, and J. D. Joannopoulos, Phys. Rev. **B54**, 7837 (1996).
 - [37] A.R. McGurn, Chaos, **13**, 754 (2003); J. Phys.: Condens. Matter **16**, S5243 (2004).
 - [38] A.E. Miroshnichenko, S.F. Mingaleev, S. Flach, and Yu.S. Kivshar, Phys. Rev. **E71**, 036626 (2005).
 - [39] A.E. Miroshnichenko and Yu.S. Kivshar, Phys. Rev. **E72**, 056611 (2005).
 - [40] S.F. Mingaleev, A.E. Miroshnichenko, Yu.S. Kivshar, and K. Busch, Phys. Rev. E **74**, 046603 (2006).
 - [41] S. Longhi, Phys. Rev. **B75**, 184306 (2007).
 - [42] A.E. Miroshnichenko, Yu. Kivshar, C. Etrich, T. Pertsch, R. Iliew, and F. Lederer, Phys. Rev. **A79**, 013809 (2009).
 - [43] A.E. Miroshnichenko, Phys. Rev.E **79**, 026611 (2009).
 - [44] J. von Neumann and E. Wigner, Phys. Z. **30**, 465 (1929).
 - [45] A.Z. Devdariani, V.N. Ostrovsky, and Yu.N. Sebyakin, Sov. Phys. JETP **44**, 477 (1976).
 - [46] H. Friedrich and D. Wintgen, Phys. Rev. **A32**, 3231 (1985).
 - [47] E.N. Bulgakov, K.N. Pichugin, A.F. Sadreev, and I. Rotter, JETP Lett. **84**, 508 (2006).
 - [48] A.F. Sadreev, E.N. Bulgakov, K.N. Pichugin, I. Rotter, and T.V. Babushkina, in book "Quantum Dots, Research, Technology and Applications", ed. By R.W. Knoss, pp. 547-577 (2008, Nova Sciencers Publ. Hauppauge, NY).
 - [49] D.R. Tilley, J. Tilley, *Superfluidity and Superconductivity* (Van Nostrand Reinhold Co. N.Y. 1974).
 - [50] S.F. Mingaleev, Yu.S. Kivshar, and R.A. Sammut, Phys. Rev. **E62**, 5777 (2000).
 - [51] S. F. Mingaleev, A. E. Miroshnichenko, and Y. S. Kivshar, Opt. Express **15**, 12380 (2007); *ibid* **16**, 11647 (2008).
 - [52] D. Michaelis, U. Peschel, C. Wächter, and A. Bräuer, Phys. Rev. **E68**, 065601R (2003).

- [53] G. Lecamp, J.P. Hugonin and P. Lalanne, Opt. Express **15**, 11042 (2007).
- [54] P. Exner, P. Šeba, A.F. Sadreev, P. Středa, and P. Feher, Phys. Rev. Lett. **80**, 1710 (1998).
- [55] G.S. McDonald and W.J. Firth, J. Mod. Optics **37**, 613 (1990).
- [56] Y. Chen, A.W. Snyder, and D.N. Payne, IEEE J. Quantum Electron. **28**, 239 (1992).
- [57] N. Boumaza, T. Benouaz, A. Chikhaoui, and A. Cheknane, Int. J. Phys. Sciences **4**, 505 (2009).
- [58] V. Grigoriev and F. Biancalana, Opt. Lett. **36**, 2131 (2011).
- [59] E.N. Bulgakov and A.F. Sadreev, J. Phys.: Cond. Mat. **23** 315303 (2011).
- [60] E.N. Bulgakov and A.F. Sadreev, Phys. Rev. B **84**, 155304 (2011).
- [61] D.C. Hutchings and B.S. Wherrett, Phys. Rev. B **50**, 4622 (1994).
- [62] A. Rodriguez, M. Soljačić, J. D. Joannopoulos, and S.G. Johnson, Optics Express **15**, 7303 (2007).
- [63] D. Milam, Appl. Optics **37**, 546 (1998).
- [64] G. Boudebs and K. Fedus, J. Appl. Phys. **105**, 103106 (2009).
- [65] Y.H. Wen, O. Kuzucu, T. Hou, M. Lipson, and A.L. Gaeta, Opt. Lett. **36**, 1413 (2011).
- [66] S.G. Johnson, C. Manolatou, S. Fan, P. R. Villeneuve, J.D. Joannopoulos, and H.A. Haus, Opt. Lett. **23**, 1855 (1998).
- [67] M. L. L. de Guevara, F. Claro, and P.A. Orellana, Phys. Rev. B **67**, 195335 (2003).
- [68] E.N. Bulgakov and A.F. Sadreev, Phys. Rev. B **80**, 115308 (2009).